Electrolyte Developments for All-Solid-State Lithium Batteries: Classifications, Recent Advances and Synthesis Methods
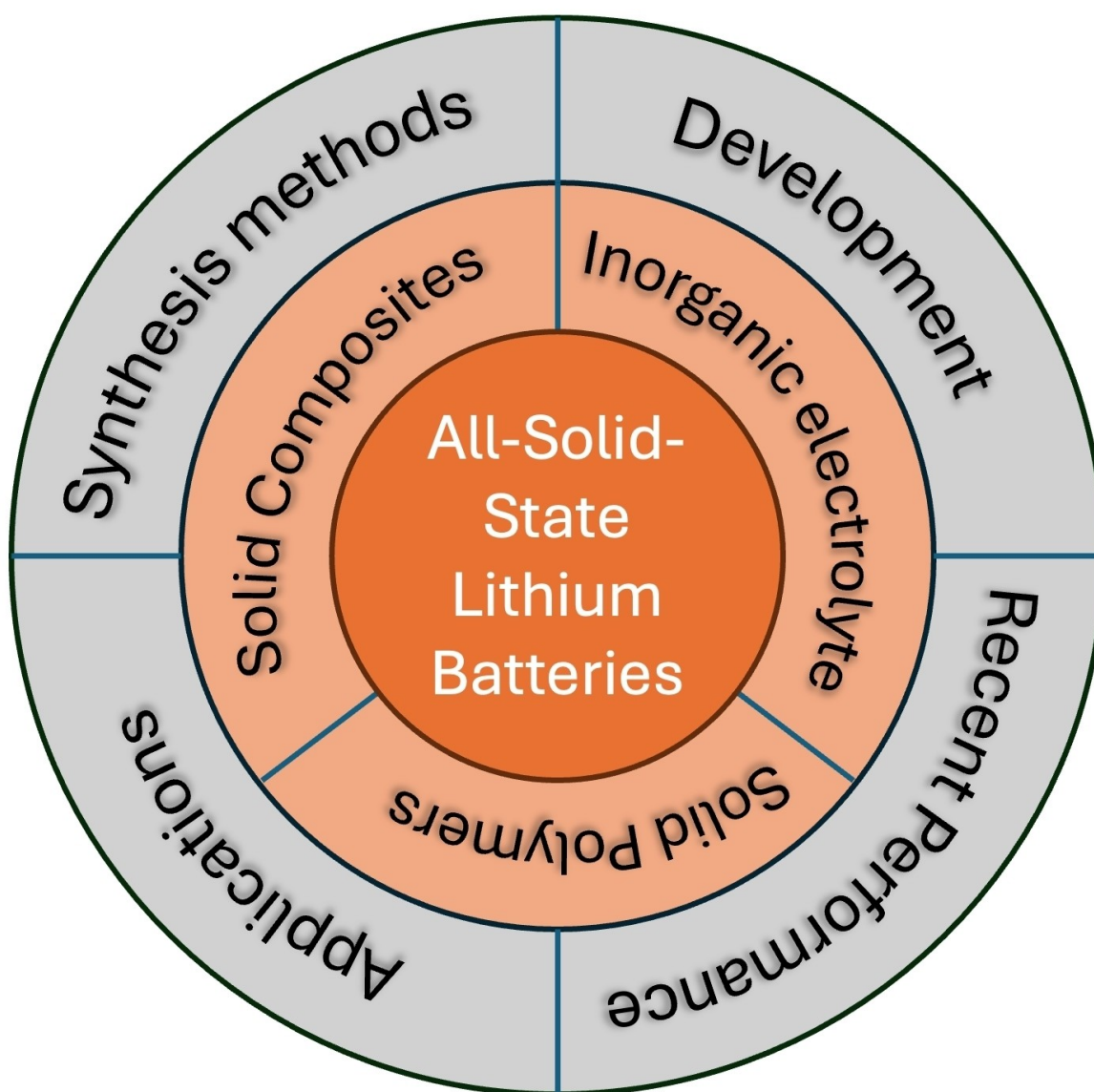
Cheuk Hei Chan,[a] Hon Ho Wong,[a] Shipeng Liang,[b, c] Mingzi Sun,[a] Tong Wu,[a] Qiuyang Lu,[a] Lu Lu,[a] Baian Chen,[a] and Bolong Huang*[a, b, d]

Batteries & Supercaps

Review
doi.org/10.1002/batt.202400432

Chemistry
Europe

European Chemical
Societies Publishing

The developments of all-solid-state lithium batteries (ASSLBs) have become promising candidates for next-generation energy storage devices. Compared to conventional lithium batteries, ASSLBs possess higher safety, energy density, and stability, which are determined by the nature of the solid electrolyte materials. In particular, various types of solid electrolyte materials have been developed to achieve similar or even superior ionic conductivity to the organic liquid electrolyte at room temperature. Although tremendous efforts have been devoted to the mechanistic understanding of solid electrolyte materials, the unsatisfactory electrochemical and mechanical performances limit the commercialization and practical application of ASSLBs. To further improve their performances, the current developments of different advanced solid electrolytes and their performances are highly significant. In this review, we summarize the comprehensive performance of the common solid electrolytes and their fabrication strategies, including inorganic-based solid electrolytes, solid polymer electrolytes, and composite solid electrolytes. The performances of the ASSLBs constructed by different solid electrolytes have been systematically compared. The practical challenges of ASSLBs will also be summarized in this review. This review aims to provide a comprehensive review of the current developments of solid electrolytes in ASSLBs and discuss the strategies for advanced solid electrolytes to facilitate the future commercialization of ASSLBs.

1. Introduction

Modern human activities and the development of science require tremendous energy consumption, and the reliance on traditional fossil fuel resources has caused severe environmental pollution issues. Meanwhile, the electrical energy generated by renewable sources such as solar, wind, and hydropower are good alternatives to replace the burning of fossil fuels. Hence, it is believed that electricity power and the corresponding energy storage technologies will play a vital role in achieving a sustainable future. Storing electrical energy in the form of chemical energy has the advantage of high conversion efficiency and energy density.[1] For example, the Lithium-ion battery (LIB) is one of the most widely used rechargeable batteries in the world owing to its high energy density (200–250 Wh/kg), wide electrochemical window (3.7–4.2 V), low cost, and limited self-discharge rate (1–2% per month). Since the first commercial LIB released by the Sony and Asahi Kasei teams in 1991, the LIBs have been applied in every aspect of our lives, leading to rapid battery market growth in the past few decades.[2] Goodenough, Whittingham, and Yoshino equally share the 2019 Nobel Prize in Chemistry for their contributions to developing Li-ion batteries due to the importance of storing electrical energy in batteries.[3] On the other hand, Li-air batteries have also attracted worldwide attention due to their high theoretical specific energy (11,140 Wh/kg). The Li-air batteries utilize the reduction and oxidation reaction between the Li metal and air (O_2/CO_2) to generate electricity. In general, the Li-air battery is composed of a Li metal as the anode, and a porous cathode is used to allow the electrochemical contact between air and Li ions in the electrolyte. While a Li-ion conductive natural organic polymer could be used as the electrolyte membrane for the Li-air batteries. Although it possess promising specific energy, the Li-air batteries are still facing various challenges which limit the performance and durability of the Li-air batteries. Fortunately, significant progress has recently been made in developing Li-air batteries. For example, Min et al.[4] demonstrated a novel design strategy to construct a rechargeable Li-O_2 battery with excellent humidity resistance, using the water-defendable protective layer to prevent water ingress on the Li anode surface. Meanwhile, the high charge overpotential and Li dendrite growth are the main issues limiting the performance of Li-CO_2 batteries. This challenge can be resolved by employing the 1-ethyl-3-methyl-imidazole bromide (EMIBr) as a defense donor redox mediator (RM).[5] At the same time, the formation of superoxide radicals ($O_2^{\bullet-}$) and the resulting deterioration of electrolytes and oxidation of the carbon cathode have also been investigated systemically in the latest study, in which both density functional theory (DFT) and experimental results indicated that the introduction of sodium lignosulfonate (LSS) as an electrolyte additive could effectively capture $O_2^{\bullet-}$ and improved the performance of the Li-CO_2 batteries.[6] Based on these latest studies, the Li-air batteries possess great potential for the next-generation energy storage system. Like the LIBs, the SEs can also replace the liquid electrolytes for Li-air batteries, forming the solid-state Li-air batteries (SSLABs) with high safety, high energy density, and environmental friendliness.

Conventional LIBs are constructed by a carbon/graphite anode, a metal oxide cathode, a separator, and organic liquid electrolytes. However, the need for a better LIB has never been terminated, especially conventional liquid electrolyte-based LIBs. Due to the highly volatile and flammable organic liquid electrolytes, conventional liquid electrolyte-based LIBs possess a potential safety risk of fire and explosion.[7] LIB constructed by organic liquid electrolytes also suffers from narrow electrochemical windows and poor thermal stability. Therefore, storing electrical energy with improved safety and electrochemical

[a] C. Hei Chan, H. Ho Wong, M. Sun, T. Wu, Q. Lu, L. Lu, B. Chen, B. Huang
     Department of Applied Biology and Chemical Technology, The Hong Kong Polytechnic University, Hung Hom, Kowloon, Hong Kong SAR, China
     E-mail: bhuang@polyu.edu.hk

[b] S. Liang, B. Huang
     CAS Center for Excellence in Nanoscience, Beijing Institute of Nanoenergy and Nanosystems, Chinese Academy of Sciences, Beijing 100083, P. R. China

[c] S. Liang
     School of Nanoscience and Technology, University of Chinese Academy of Sciences, Beijing 100049, P. R. China

[d] B. Huang
     Research Centre for Carbon-Strategic Catalysis, The Hong Kong Polytechnic University, Hung Hom, Kowloon, Hong Kong SAR, China

Batteries & Supercaps

Review
doi.org/10.1002/batt.202400432

Chemistry Europe
European Chemical
Societies Publishing

performance is crucial. All-solid-state lithium batteries (ASSLBs) with solid electrolytes (SEs) are the perfect solution to address conventional liquid electrolyte-based LIB safety and performance issues.[8] Compared with the highly flammable liquid electrolyte, nonflammable SEs not only greatly enhance the safety of the batteries but also have the advantage of better durability, wider electrochemical windows, and higher energy and power density.[9] As a result, ASSLBs with SEs have received worldwide attention as next-generation electrical energy storage devices, and the advances in SE developments have determined the revolution of ASSLB technologies. On the other hand, some challenges of the ASSLBs, such as the cost, interfacial resistance, scalability, and compatibility, need to be addressed for further development. These challenges limit the development and applications of ASSLBs in different fields.

The ASSLBs are constructed by three main components: the cathode, solid-state electrolyte (SE), and anode. In contrast with the conventional LIBs, both the cathode and anode are immersed in the liquid electrolyte with a separator to prevent the liquid on the cathode side from mixing suddenly with the liquid on the anode side, the SE directly separates the cathode and anode without the need of separator. The cathode (positive electrode) is the oxidizing electrode in the battery; hence, it should be an efficient oxidizing agent. In ASSLBs, the cathode materials must be stable and able to maintain good physical contact with the SEs. Typically, Li transition metal oxides are often used as the cathode materials for LIBs, such as lithium cobalt oxide (LCO), Li manganese oxide (LMO), lithium nickel manganese cobalt oxide (NMC), and Li nickel cobalt aluminum oxide (NCA).[10] Meanwhile, cost-effective carbon materials with good electrical conductivity, including carbon black (CB), carbon nanotubes (CNTs), graphene, and carbon nanofibers (CNF), can also incorporated as conductive materials into the cathode to further enhance the electrical conductivity of Ni-rich cathode material, forming the composites electrode.[11] Meanwhile, the intercalation-type or conversion-type cathode active materials (CAMs) have been adopted to improve the specific capacity and cyclability of ASSLBs. For the anode, the Li metal is the most used anode material for ASSLBs, but the side reactions between the metallic Li anode and electrolyte reduce the battery performances and significantly hamper the implementation of Li anodes. The Si ($Li_{15}Si_4$) is one of the most promising anode materials for achieving a high energy density and safe operation of ASSLBs due to its high specific capacity, abundant reserves, and high working potential.[12] The working principle of ASSLBs is similar to that of the conventional LIBs, in which the ASSLBs consist of an SE in place of a liquid electrolyte, but the function of SE in ASSLBs is the same as the liquid electrolyte in conventional LIBs. On discharge, the anode undergoes oxidation, and the cathode is reduced, accompanied by the migration of Li-ion from the anode to the cathode through the Li-ion conducting SEs. During charge, this process is reversed, in which the Li-ion moves from cathode to anode and passes through the SEs for the rechargeable battery.

Depending on the materials, the Li-ion conducting SEs for ASSLBs can be classified into three main categories: (i) inorganic-based SEs,[13] (ii) organic polymer-based SEs,[14] and (iii) composite SEs.[15] Although SEs made from various materials would have different physical and chemical properties, they mostly share the same working principle during the charge/discharge process of the battery. When ASSLB charges, the Li-ions de-intercalate from the cathode and transfer to the anode via the Li-ion conductive SE, while the electron moves from the cathode to the anode via an external circuit. During the discharging process, the Li-ions move reversely from the anode to the cathode through the SEs, and electrons are passed through the external circuit, which drives a device to work.[16] Therefore, the key point for making good SEs next-generation rechargeable ASSLBs is to achieve high Li-ion conductivity, which the ionic conductivity of SEs greatly determines battery capacity and charge/discharge rate, especially the ionic conductivity at room temperature. Besides Li-ionic conductivity, another key feature is the solid-solid interface between the electrode and the SEs.[17] The reaction steps in the electrolyte-electrode interface involve (i) Li diffusion in the electrolyte, (ii) adsorption on the electrode surface, (iii) charge transfer, (iv) intercalation into the electrode, (v) Li diffusion in the electrode, and (vi) surface reaction. Moreover, the chemical and physical interaction between the electrolytes and electrode may also cause poor thermal stability due to undesired side reactions at the interface. For instance, the growth and expansion of Li dendrite will cause internal short circuits and significantly reduce the safety properties of batteries. Besides conductivity and stability, the electrochemical window (EW) is another crucial consideration for SEs. SEs with a wide electrochemical window can reduce undesirable electronic transport, including charge injection or extraction from electrodes, such as self-discharge or short-circuiting. In addition, a wide electrochemical window also guarantees the high energy density of the ASSLBs. In summary, an ideal SEs for ASSLBs should possess the following features: (i) High ionic conductivity at room temperature with fast ionic dynamic and negligible electronic conductivity; (ii) wide electrochemical window against the electrodes for high energy density and long-term durability of the ASSLBs; (iii) excellent mechanical strength, thermal and electrochemical stability; (iv) low-cost and easy to fabricate for large-scale applications.[18]

Dr. Bolong Huang is an Associate Professor at the Department of Applied Biology and Chemical Technology and Director of the Research Centre for Carbon-Strategic Catalysis. His main research fields are electronic structures of nanomaterials, energy materials, solid functional materials, and rare earth materials, as well as their applications in multi-scale energy conversion and supply systems. Dr. Huang has published 329 research papers and has received citations over 25000 times with h-index of 88. He is the Associate Editor of Battery Energy and Frontiers in Chemistry, the Early Career Advisory Board of JACS Au, and Young Star Editor of Nano Research.

Batteries & Supercaps

Review
doi.org/10.1002/batt.202400432

Chemistry Europe
European Chemical
Societies Publishing

Since the invention of ASSLBs, the primary target has always been to maximize the gravimetric and volumetric energy density of the battery cell unit. Currently, the ASSLBs made by oxide-, halide-, sulfide-, and polymer-based and composite SEs can achieve high energy density paired with the Li anode. Although the current representative SEs for ASSLBs can exhibit an ionic conductivity comparable with traditional liquid electrolytes, the ASSLBs that can work stably under ambient conditions with high energy and power density are still lacking in the report.[19] This poor electrochemical performance of the ASSLBs at room temperature can be attributed to the low ionic conductivities of the SEs at room temperature, especially for the organic-based solid polymer electrolytes. Additionally, the high interfacial resistance between inorganic-based SEs and electrodes is the main reason for the insufficient electrochemical performance of ASSLBs. Last but not least, the stability issues of the electrode also hinder the development of highly efficient ASSLBs. Owing to these challenges of ASSLBs, the investigation of SEs mainly focused on enhancing the Li-ion conductivity and improving the electrode/electrolyte interface property of the ASSLBs. In the past decade, great progress has been achieved in fabricating SEs with extraordinary Li-ion conductivity at room temperature. Followed by a better understanding of the Li-ion transportation mechanism and ionic behaviors between the electrolyte/electrode interfaces, various high-performance inorganic- and organic (polymer)-based SEs were developed for advanced ASSLBs. The present review will provide a systematic summary of the development of current SEs, including inorganic SEs, solid polymer electrolytes, and composite polymer electrolytes. Also, the fabrication strategies and performance of the ASSLBs constructed by various SEs will be introduced. Also, the fabrication strategies, performance of the ASSLBs constructed by various SEs, and the practical challenges will be introduced.

2. Inorganic Solid Electrolytes Classifications

Inorganic SEs are one of the most used SEs for ASSLBs; hence, considerable research has been devoted to optimizing the electrical and mechanical properties of inorganic SEs. Compared with the liquid electrolytes, the SEs made from inorganic material can operate under a wide temperature range (-50 to over $200\,^{\circ}C$) with no significant ionic conductivity variation owing to the low activation energies for fast-ion conduction.[20] Additionally, inorganic SEs also provide potential benefits for high potential cathode material (>5 V) and are able to achieve higher power capability because of the absence of bulk polarization on solid materials. On the other hand, the ionic conductivity of the SEs was determined by the mobility of cations (Li^+) on the solid. At the atomic level, the diffusion pathway of the cation can be visualized as the hopping of the ions between the ground-state (stable sites) and the intermediate metastable sites on the framework. Therefore, the energies of the sites and the corresponding activation energy of the ion transportation are mainly defined by the bonding and coordination environment of the ion. For example, body-centered

cubic (BCC) crystals commonly displayed fast ion conductivity because of the low activation energy required for the direct Li-ion hopping between adjacent tetrahedral sites, and the hopping through octahedral sites with higher activation energy was not necessitated.[21] For crystalline inorganic SEs, the ions migrate depending on the cationic vacancies or interstitials. The ion can migrate to a neighboring vacant site by vacancy diffusion or correlated interstitialcy mechanism. In general, the ionic conductivity of inorganic SEs increases with the temperature and is mainly regulated by the Arrhenius equation[22]:

$$\sigma = \frac{\sigma_0}{T} e^{-E_a/k_B T}$$

Where the σ_0 is the pre-exponential factor, T is the temperature in Kelvin (K), E_a is the activation energy for Li-ion diffusion and k_B is the Boltzmann constant.

2.1. Oxide-Based SEs

Li-conductive oxide materials are well-known for their excellent oxidation stability, thermal stability, and good ionic conductivity. The oxide-based SEs could display various electrical and chemical properties depending on the chemical structures. The common oxide-based SEs involved sodium superionic conductors (NASICON), crystalline perovskite (LLT and LATP), and garnet-type crystals (LLZO). However, most oxide-based SEs have high rigidity and brittleness, leading to poor physical contact and hindering ion diffusion between the SEs and the electrode.[23] Therefore, the approaches aimed at enhancing the performance of oxide-based SEs predominantly focus on improving the ionic conductivity and solving the poor mechanical properties and high interface impedance issues. The following section will briefly outline various oxide-based SEs to show their electrochemical features.

The first reported NASICON material is $Na_{1+x}Zr_2Si_xP_{3-x}O_{12}$, which exhibits high ionic conductivity for Na ions.[24] The Li superionic conductors (LISICON) for Li-ion conduction ($LiGe_xTi_{2-x}(PO_4)_3$) were devolved later based on the proposed sodium-based NASICON. The chemical formula of NASICON/LISICON-type materials is $AM_2(XO_4)_3$, in which the $[M_2X_3O_{12}]$ is the skeleton forming the basic structure. Generally, the A site in the formula is occupied by 1st-row alkali metal ions such as Li^+, Na^+, K^+, Rb^+, and Cs^+, and the M sites could be occupied by various multivalent transition metal ions (from divalent to pentavalent) to balance the charge suitably. For LISICON (e.g. $LiM_2(PO_4)_3$), the Li^+ ions should reside on the 6-fold coordinated M1 site and 6-fold coordinated M2 sites, where the M1 site is located between two stacked MO_6 units and the M2 site is located between two columns of MO_6 units. It is also worth noticing that the Li-ion conductivity of LISICON is considerably lower than sodium-based NASICON because the ion channels within the designed NASICON are unsuitable for facilitating Li-ion migration.[26] The common examples of LISICON included $LiZr_2(PO_4)_3$, $LiTi_2(PO_4)_3$, and $LiGe_2(PO_4)_3$. On the other hand, doping other elements is the most adopted strategy for tuning

Batteries & Supercaps

Review
doi.org/10.1002/batt.202400432

Chemistry Europe
European Chemical
Societies Publishing

the interstitial channel size for Li$^+$ ion diffusion for LISICON. For instance, through the doping of Y^{3+} ions, the resulting Li$_{1+x}$Y$_x$Zr$_{2-x}$(PO$_4$)$_3$ (LYZP, where $0.1 \leq x \leq 0.2$) could achieve improved bulk conductivity of 1.4×10^{-4} S cm^{-1} and Li-ion conductively of 0.71×10^{-4} S cm^{-1} due to the reduction of the M1 cavity after the Y^{3+} doping.[27] Except for the Y^{3+} ions doping, the doping of Al^{3+} in LiTi$_2$(PO$_4$)$_3$ (LTP) is also able to increase the Li-ion conductively by accommodating more Li in the structure in order to compensate for the charge balance.[28]

Crystall perovskites are another important type of Li-conductive SE for ASSLBs. The general formula for ideal perovskite is ABO$_3$, where A (6-fold oxygen-coordination) and B (12-fold oxygen-coordination) are two cations of very different sizes. In the perovskite's crystal structure, the A site is occupied by larger cations such as Na$^+$, K$^+$, Ca^{2+}, Sr^{2+}, Ba^{2+}, La^{3+}, whereas the B are cation with smaller ionic radius, such as Sc^{3+}, In^{3+}, Al^{3+}, Sm^{3+}, Ga^{3+}, Ti^{4+}, Zr^{4+}, Hf^{4+}, Sn^{4+}, Ge^{4+}, Nb^{5+}, Ta^{5+}. The space group for ideal cubic perovskites is Pm3 m, while the space group for orthorhombic and tetragonal variants are Pnma and I4/mcm, respectively. The cubic and tetragonal perovskite are the two main structures for perovskite-type SEs, and the perovskite-type SEs are mostly A-site-deficient materials.[29] There are numerous advantages for perovskite-type SEs, La$_{2/3-x}$Li$_{3x}$TiO$_3$ (LLTO) is one of the most representative perovskite-type SEs used in ASSLBs owing to its relatively high bulk ionic conductivity (~10^{-3} S cm^{-1}) at room temperature, large ionic transference numbers (0.5–0.9) and excellent chemical and thermal stability in air.[30] However, LLTO has also suffered from the issues of poor stability against Li metal anode and high interface resistance. The LLTO mostly has a tetragonal crystal structure, in which the La^{3+} is unevenly distributed at La1 and La2 sites, leading to the doubling of the c-axis cell parameter and the tilting of TiO$_6$ octahedra. Doping is the most common strategy for improving the electrochemical performance of LLTO. For example, doping large rare-earth or alkaline-earth metal ions in A site of the perovskite structure can increase the ionic conductivity. This is because the Li-ions migrate via the octahedral channels (ab plane or c-axis migration pathway), in which Li-ions predominantly migrate along the ab plane due to the bottleneck size of the c-axis being much smaller than that of the ab plane.[31] The doping of larger cations in A-sites could expand the bottleneck size, thus increasing the ionic conductivity of LLTO.[32] For the B-site, substituting a smaller cation could reduce interatomic Ti–O bond length; thus, the competing Li–O bond will be weakened, which can also increase the ionic conductivity of LLTO.[33] For interfacial stability, the Ti reduction at the LLTO/Li anode interface is a major issue. The Ti^{4+} in LLTO can react readily with Li metal anode during direct contact, resulting in the decomposition of LLTO and influencing the diffusion of Li ions in electrolytes. Moreover, Li dendrites also grow easily at the LLTO pellet voids during cycling.[34] To improve the interfacial compatibility between LLTO and Li metal anode, a feasible approach is modifying the electrolyte surface coating. Soft polymer matrix such as polyethylene oxide (PEO) can also be used as an interface protection layer for perovskite SEs to avoid the adverse Ti reduction between the LLTO and Li metal anode by preventing direct LLTO-anode

contact.[25] As a result of PEO coating, the Li|PEO-LiTFSI-LLTO|Li symmetric cell displayed superior stability, in which the battery can remain stable after 400 h of operation without short-circuiting, and with a capacity retention of 79.0% after 300 cycles at 2°C at 60°C (Figure 1). Moreover, Ti-free perovskites such as Li$_{3/8}$Sr$_{7/16}$Ta$_{3/4}$Zr$_{1/4}$O$_3$ displayed much better anode compatibility and Li dendrites suppression due to the avoiding of Ti reduction.[35]

Garnet-type oxide (A$_3$B$_2$C$_3$O$_{12}$) SEs are excellent Li-ion conductors with high ionic conductivity (~ 10^{-3} to 10^{-4} S/cm), wide electrochemical windows, and excellent chemical stability with negative Li metal electrodes.[36] Currently, the most used garnet-type oxide SE is Li$_7$La$_3$Zr$_2$O$_{12}$ (LLZO) owing to its excellent comprehensive performances, including high room temperature Li-ion conductivity because of its high lithium content compared with other electrolytes.[36b] However, several issues still exist for the practical garnet-type oxide SE applications, such as the ionic conductivity of garnet-type oxide SEs is still lower than the liquid electrolyte. Additionally, the interfacial issues between solid electrolytes and electrodes are another major drawback of LLZO, leading to high interfacial resistance and inhomogeneous current distribution.[37] The poor air stability of garnet-type oxide SEs due to the formation of Li$_2$CO$_3$ in the surface under the atmosphere also leads to the degradation of ionic conductivity and increased interfacial resistance.[38] These problems have limited the wider use of garnet-type oxide SEs for ASSLBs, while different strategies were developed to encounter these issues of garnet-type oxide SEs. To further improve the ionic conductivity of LLZO, it is important to effectively control the chemical stoichiometry and Li$^+$ concentration in LLZO to obtain high ionic conductivity. Due to the volatile nature of Li, low-temperature sintering should be adopted to reduce the loss of Li$^+$ concentration.[39] In addition, the crystal structure of LLZO also plays an important role in Li-ion conduction. LLZO generally has two kinds of skeleton-like phase structures: tetragonal (t-LLZO) and cubic (c-LLZO).[40] The ionic conductivity of c-LLZO is about two orders of magnitude higher than the t-LLZO due to the difference in Li$^+$ arrangement. Therefore, the formation and stabilization of c-LLZO are the key to enhancing its ionic conductivity. Meanwhile, the sintering condition also greatly affects the LLZO crystallization and the ionic conductivity. Kim et al.[41] found that the optimal temperature for the c-LLZO formation was estimated to be 600°C, in which both bulk and grain boundary ionic conductivities were improved (1.87×10^{-4} S cm^{-1}). For the cathode/LLZO interface, the stability of LLZO with cathode material was investigated by computational studies. The study demonstrated that the LiCoO$_2$ (LCO)/LLZO is the most stable interphase owing to the lowest driving force for the LCO decomposition in the charge state, whereas other cathodes such as LMO and LFP react strongly with the LLZO.[42] Nevertheless, side reactions frequently occur, creating a secondary phase (insulating layer) on LLZO under humid air, contributing to interfacial resistance and negatively affecting the capacity at room temperature. The LCO/LLZO interface issues can be solved by employing the co-sintering for the LCO cathode with Nb-doped LLZO (LLZO–Nb), in which the side reaction between the
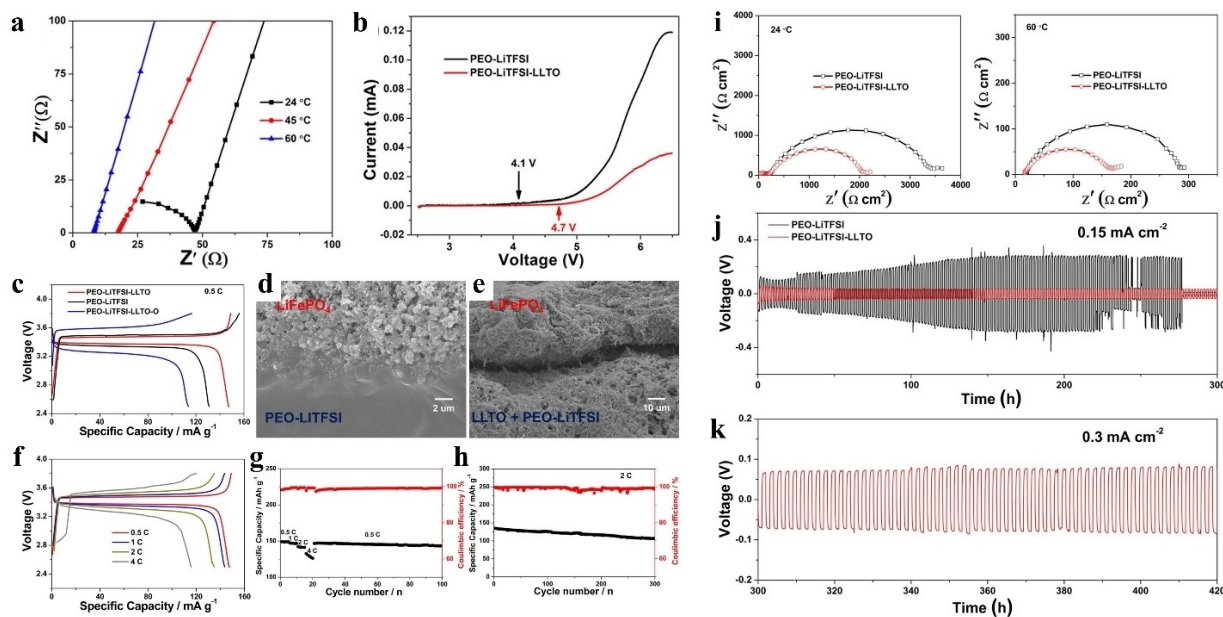
Batteries & Supercaps

Review
doi.org/10.1002/batt.202400432

**Chemistry
Europe**
European Chemical
Societies Publishing

Figure 1. (a) EIS profiles of the PEO|PEO-perovskite|PEO SE at different temperatures. (b) Linear sweep voltammetry (LSV) of the electrolyte and PEO-LiTFSI. (c) The charge-discharge voltage profiles of Li/PEO-LiTFSI-LLTO/LiFePO$_4$, Li/PEO-LiTFSI/LiFePO$_4$, and Li/PEO-LiTFSI-LLTO—O/LiFePO$_4$ batteries at 0.5 °C and 60 °C. (d, e) The cross-sectional SEM image of the interface. (f) The charge-discharge voltage profiles of the Li/PEO-LiTFSI-LLTO/LiFePO$_4$ battery at different rates at 60 °C. (g) Rate performance of the Li/PEO-LiTFSI-LLTO/LiFePO$_4$ battery at 60 °C. (h) Cycling performance of the Li/PEO-LiTFSI-LLTO/LiFePO$_4$ battery at 2 C at 60 °C. (i) The impedance spectra of the Li/PEO-LiTFSI/Li and Li/PEO-LiTFSI-LLTO/Li symmetric cells at 24 and 60 °C. (j) Voltage profiles of the symmetric cells cycling at 60 °C. (k) Voltage profile of the continued cycling of the Li/PEO-LiTFSI-LLTO/Li symmetric cell at 0.3 mA cm^{-2} at 60 °C. Reproduced with permission.[25] Copyright 2019 ACS.

LCO and LLZO–Nb can be greatly suppressed at low sintering temperatures.[43] In addition, coating the LLZO layer on the cathode materials also could improve the interface stability.[44] For example, the coating of uniform thin LLZO on the Li$_{1.2}$Mn$_{0.54}$Ni$_{0.13}$Co$_{0.13}$O$_2$ (S-LLNCM) submicron particles, in which LLZO not only acts as a protective layer to inhibit the adverse reactions at the interface but also provides an ionic conductive pathway that facilitates the interfacial Li$^+$ diffusion.[45] For the interfacial issue between LLZO and Li-metal (anode), interface medication can be adopted to improve the physical contact and wettability of LLZO with Li anode via the formation of Li-alloy and conversion of solid electrolyte's surface wettability from lithiophobicity to lithiophilicity. For instance, ultrathin lithiated Si coating can change the wettability properties of garnet LLZO from "super-lithiophobicity" to "super-lithiophilicity", which the lithiated Si coating acts as a Li-ion conductor layer and lowing the interfacial resistance with improved Li metal/LLZ interface contact.[46] For air stability issues, the LLZO tends to react with the moisture and CO$_2$ in the atmosphere, leading to impurities formation of LiOH and Li$_2$CO$_3$.[38] The doping of Al^{3+} into LLZO could result in Al-doped LLZO pellets with small grains that are more stable than those with large grains, due to the distribution differences of Al and Li-ions on the surface of Al-doped LLZO.[47]

Murugan et al.[36b] reported the Li$_7$La$_3$Zr$_2$O$_{12}$ (LLZ) based garnets with ionic conductivity of 5.0×10^{-4} S cm^{-1} at room temperature, which became the benchmark of garnet-based solid-state electrolytes. While the representative oxide-based

SEs included LLZO such as Li$_{6.55}$Ga$_{0.15}$La$_3$Zr$_2$O$_{12}$ with room temperature ionic conductivity of 2.1×10^{-3} S cm^{-1}, and LATP such as Li$_{1.3}$Al$_{0.3}$Ti$_{1.7}$(PO$_4$)$_3$ with room temperature ionic conductivity of 7.0×10^{-4} S cm^{-1}.[48] In addition, a new type of oxide SEs based on Li$_{29}$Zr$_9$Nb$_3$O$_{40}$ (LZNO) was reported in 2020.[49] The pure LZNO shows a bulk ionic conductivity of 1.75×10^{-4} S cm^{-1} and a total conductivity of 5.90×10^{-5} S cm^{-1} at room temperature, while the Al-modified LZNO has an improved ionic conductivity of 2.41×10^{-4} S cm^{-1}. These representative oxide-based SEs are served as the benchmark SEs for ASSLBs.

2.2. Sulfide-Based SEs

Besides the oxide-based SEs, sulfide-based SEs have also been widely studied as a common Li-ion conducting material. Unlike the hard and brittle oxide-based SEs, the sulfide-based SEs are relativity "soft" with better interfacial contact.[50] Additionally, due to their favorable plastic properties, sulfide-based SEs can easily reduce grain-boundary resistance via conventional cold-pressing of the electrolyte powder. As a result, sulfide-based SE powders are one of the most promising candidates for the construction of ASSLBs.[51] The early research on sulfide-based SEs mainly focuses on glassy materials (such as Li$_2$S-P$_2$S$_5$-LiI, B$_2$S$_3$-Li$_2$S-LiI, Li$_2$S-SiS$_2$-GeS$_2$, and Li$_3$PS$_4$), but these early glassy sulfide-based SEs exhibited relatively low ionic conductivity.[52] Reducing the grain-boundary resistance by hot pressing could greatly increase the ionic conductivity of the glassy Li$_2$S-P$_2$S$_5$

Batteries & Supercaps

Review
doi.org/10.1002/batt.202400432

**Chemistry
Europe**
European Chemical
Societies Publishing

glass-ceramic to about 17 mS cm^{-1}.[53] Furthermore, Li argyrodites are also a popular type of sulfide electrolyte that is able to reach high ionic conductivity of over 10 mS cm^{-1}. For example, the Li$_{5.5}$PS$_{4.5}$Cl$_{1.5}$ prepared by the ultimate-energy mechanical alloying method exhibited a high ionic conductivity of 10.2 mS cm^{-1}.[54] Recently, a new type of Ge-substituted thio-antimonate iodide argyrodite SEs was synthesized by a high-energy ball milling method with extremely high ionic conductivity and outstanding air stability.[55] The synthesized Li$_{6.5}$Sb$_{0.5}$Ge$_{0.5}$S$_5$I displays a high ionic conductivity of 16.1 mS cm^{-1}, attributed to the concerted migrations of Li-ions through the inter-cage pathways, significantly enhancing ionic conductivity. On the other hand, the Li$_{10}$GeP$_2$S$_{12}$ (LGPS)-type SE is well-known for its remarkable ionic conductivity (12 mS cm^{-1}).[56] This exceptional performance of LGPS is primarily due to its unique crystal structure, which facilitates rapid Li-ion transport.[57] This also is the first reported sulfide-based SEs that exhibited room-temperature ionic conductivity exceeding that of liquid electrolyte. In addition, by leveraging the unique properties of high-entropy materials, researchers have recently developed a monophasic LSiM$_8$PSBrO (M=Ge, δ = 0.4) with bulk ionic conductivity of 32 mS cm^{-1} at room temperature, marking the highest conductivity among the ASSLB reported to date.[60]

Since the sulfide-based SEs can be constructed by more than one phase, the sulfide-based SEs can be divided into three systems: (i) the pseudo-binary, (ii) the pseudo-ternary, and (iii) the pseudo-quaternary.[61] Examples of the pseudo-binary sulfide-based SEs include the typical Li$_2$S-P$_2$S$_5$ and Li$_2$S-MS$_2$ systems, while the ionic conductivity of the pseudo-binary sulfide-based SEs is usually lower than the pseudo-ternary and pseudo-quaternary sulfide-based SEs. In contrast, the pseudo-ternary system included Li$_2$S-P$_2$S$_5$-MS$_2$ (where the M=Ge, Si, Sn, Al, etc.) with a thio-LISICON (Li Super Ionic conductor) structure, and Li$_2$S-P$_2$S$_5$-LiX (where X=F, Cl, Br, and I) with an argyrodite structure. Generally, the pseudo-ternary sulfide-based SEs display higher ionic conductivity than the pseudo-binary system. On the other hand, pseudo-quaternary sulfide SEs can usually achieve higher ionic conductivity than pseudo-binary and pseudo-ternary sulfide-based SEs. One of the examples of pseudo-quaternary sulfide SEs is Li$_{9.54}$Si$_{1.74}$P$_{1.44}$S$_{11.7}$Cl$_{0.3}$, which exhibited ultra-high ionic conductivity (25 mS cm^{-1}) and excellent electrochemical stability.[62]

Important sulfide-based SEs, such as LGPS, LSPSCl, and Li$_6$PS$_5$B, usually display a high ionic conductivity of over 1.0×10^{-3} S cm^{-1}. For example, the representative sulfide-based SEs included Li$_{10}$GeP$_2$S$_{12}$, which gives the benchmark for the novel sulfide-based SEs for ASSLBs.[63] The Li$_{10}$GeP$_2$S$_{12}$ exhibited a high ionic conductivity of 1.6×10^{-3} S cm^{-1} and electronic conductivities of 9.8×10^{-9} S cm^{-1} at room temperature. Recently, Fan et al.[64] proposed a dual anionic novel sulfide-based SEs Li$_{6.58}$P$_{2.76}$N$_{0.03}$S$_{10.12}$F$_{0.05}$ with superior room temperature ionic conductivity of 4.33×10^{-3} S cm^{-1} as well as lowest bulk electronic conductivity of 4.33×10^{-10} S cm^{-1}, which set a new benchmark performance for ASSLBs with the superior critical current density of 0.90 mA cm^{-2} at room temperature.

2.3. Halide-Based SEs

The metal halide SEs with the general formula Li–M–X (where M is a metal element and x is the halogen) are considered to be a promising candidate for enabling ASSLB technology.[65] In contrast with divalent chalcogen (e.g. sulfide) anions, the monovalent halogen anions have a weaker Coulombic force with Li-ions during ion migration, which leads to a faster Li-ion transport kinetic and hence possible to achieve higher ionic conductivity for halide-based SEs. Nevertheless, the ionic radii of halogen anions (167 pm to 202 pm) are also larger than oxide (126 pm) as well as sulfide anions (170 pm), leading to better ion mobility and deformability due to the longer ionic bond lengths in halide-based SEs. Despite the numerous potential advantages of metal halide SEs, the early-developed halide-based SEs cannot be applied in practice due to their extremely low Li-ionic conductivity at room temperature.[66] Another issue for most halide-based SEs is that they are deliquescent substances sensitive to moisture due to the hygroscopic nature of halides.[67] Hence, designing air-stable metal halide materials with high ionic conductivity for ASSLBs is the major research direction for halide-based SEs. The trigonal Li$_3$YCl$_6$ and monoclinic Li$_3$YBr$_6$ have first demonstrated that halide-based SEs could have decent room-temperature ionic conductivity.[65a] However, these halide-based SEs still suffer from poor air stability, low electrochemical reduction stability, and limited high-voltage compatibility. Owing to the relatively higher redox potential of the halide compared to oxide and sulfide, the halide-based SEs also could possess higher oxidative stability and a wider electrochemical stability window.[68] In particular, fluoride has the highest oxidation stability (oxidation stability: F$^-$ > Cl$^-$ > Br$^-$ > I$^-$) as well as the widest electrochemical stability window.[69] However, the room-temperature ionic conductivities of fluoride-based SEs (e.g. LiMF$_4$) are insufficient for practical applications.[70] The fluoride- and chloride-based SEs are a good choice for high-voltage transition metal oxides due to their wide electrochemical stability window. In contrast, the halide-SEs based on bromide and iodide can be used for developing solid-state Li–S and Li–O$_2$ batteries because of the suitable battery operating voltage.[71]

For the structure of halide-based SEs, the ionic radius ratio of cations to anions (r$^+$/r$^-$) must meet certain conditions to form a stable lattice structure.[72] Based on the law of ionic packing, the most common form of fluoride-based SEs is the LiMF$_4$ phase with the trivalent M^{3+} cation occupying the cubic site of the F$^-$ (ionic radius = 122 pm) framework (MF$_8$ cube), as the radius ratio of M^{3+}/F$^-$ is usually needs to greater than 0.732. For the chloride (Cl$^-$, 167 pm), bromide (Br$^-$, 182 pm), and iodide (I$^-$, 202 pm)-based SEs, the trivalent M^{3+} cation tends to form MX$_6$ octahedron coordination with Li$_3$MX$_6$-type structure, as radius ratio is often between 0.414 and 0.732. Besides, the ion transport kinetic and coordination environment of metal halide SEs (Li–M–X) are controlled by their halide anion sublattice, in which different anion sublattices lead to different ion transport pathways.[73] For Li–M–X ternary halides, the sublattice structures included hexagonal close-packing (hcp: trigonal and orthorhombic) and cubic close-packing (ccp:

Batteries & Supercaps

Review
doi.org/10.1002/batt.202400432

Chemistry Europe
European Chemical
Societies Publishing

Monoclinic). For hcp anion lattices like Li_3YCl_6, the Li^+ ions transportation occurs through an anisotropic 3D diffusion network with fast one-dimension (1D) diffusion channels along the c-axis, whereas the ccp anion lattices such as Li_3YBr_6, the 3D diffusion network is isotropic.[68b] Because of different ion diffusion between the hcp and ccp framework, the ccp-monoclinic displays much higher ionic conductivity than trigonal and orthorhombic halide SSEs with an hcp framework (general trend of ionic conductivity: ccp-monoclinic > hcp-orthorhombic > hcp-trigonal).[74] At the same time, the ionic conductivity of the halide-based SEs can be enhanced by tuning the lattice structures. In particular, since the hcp anion sublattices have an anisotropic ion diffusion network with fast c-axis ion transport, the ion transport in the z-direction is likely to be the rate-determining step. Hence, the ionic conductivity of halide-based SEs with the hcp framework can be improved by increasing the disorder of Y2 and Y3 sites in the z-direction. The relatively low ionic conductivity of the hcp framework could be improved via aliovalent substation by trigonal and orthorhombic structure changes to a new orthorhombic structure (orthorhombic-II). For example, the substitution of M by Zr on $Li_3M_1Cl_6$ (M=Y, Er, and Yb) metal halide SEs led to a

significant improvement in ionic conductivity (up to 1.4 mS cm^{-1} at 25 °C) and oxidation stability (> 4.0 V) due to the trigonal-to-orthorhombic phase transition (Figure 2).[58,59] Additionally, introducing micro-strain and stacking faults during the synthesis process also helps facilitate the Li-ion transport and increase the ionic conductivity of halide SEs with hcp anion sublattice.[75] For against the moisture environments, structural tuning combined with surface coatings could significantly improve the moisture stability of halide-based SEs.[76]

Overall, Li_3YCl_6 and Li_3YBr_6 are the two important halide-based SEs that represent the revival of halide-based SEs. These benchmark SEs exhibited room temperature Li-ion conductivity of 5.1×10^{-4} S cm^{-1} and 1.7×10^{-3} S cm^{-1} for Li_3YCl_6 and Li_3YBr_6, respectively. On the other hand, most of the recently developed halide-based SEs have an ionic conductivity close to 10^{-3} S cm^{-1} level due to the grain boundary reduction. For example, the Li_3InCl_6 reported by Li et al. demonstrated good stability against moisture in the air and exhibited a high ionic conductivity of 2.04×10^{-3} S cm^{-1} at room temperature.[77] This novel halide-based SE is also electrochemically stable with high-voltage oxide cathodes, proving that the Li_3InCl_6 is a highly promising
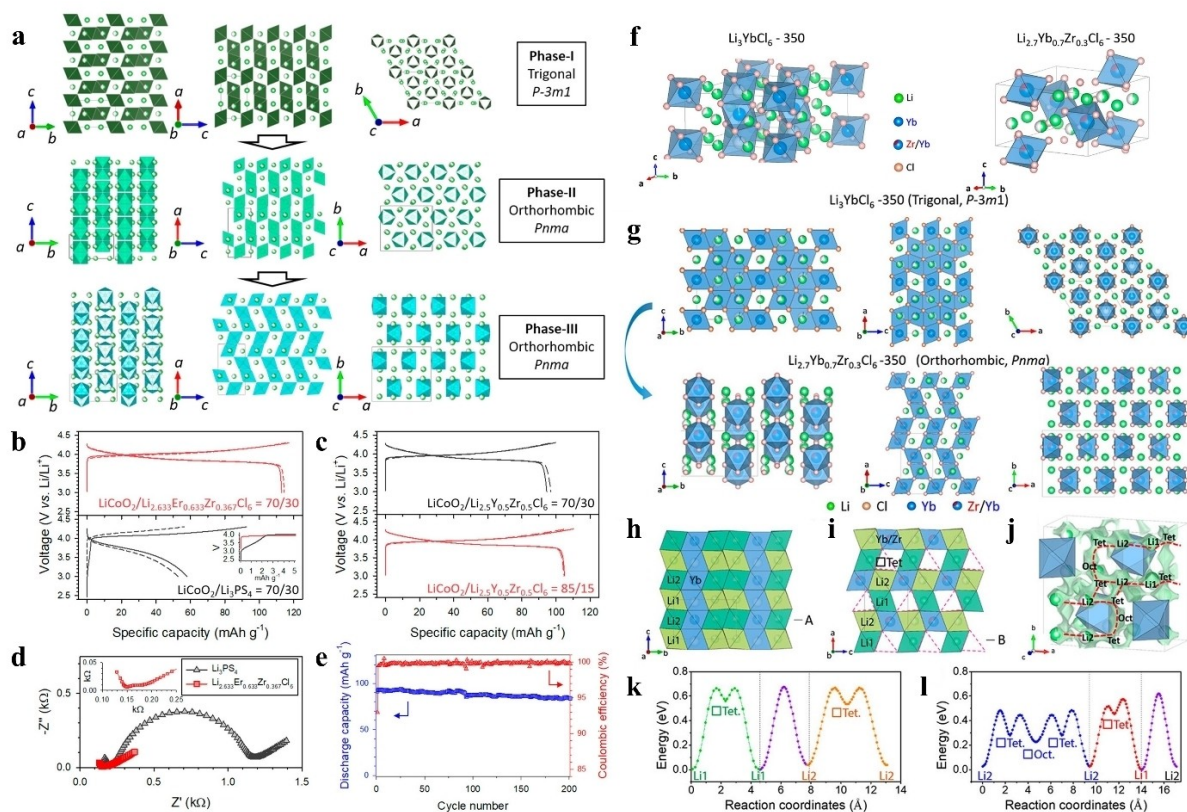

Figure 2. (a) Phase evolution of $Li_3M_{1-x}Zr_xCl_6$ (M=Er, Y) upon Zr substitution. The first (solid) and second (dashed) charge-discharge voltage profiles of LiCoO$_2$/chloride-SE│Li$_3$PS$_4$│Li$_{11}$Sn$_6$ cells using (b) $Li_{2.633}Er_{0.633}Zr_{0.367}Cl_6$, Li$_3PS_4$, and (c) $Li_{2.5}Y_{0.5}Zr_{0.5}Cl_6$ as the solid electrolyte in the cathode composite at a current density of 0.11 mA cm^{-2} (~0.1 °C). (d) Nyquist plots of LiCoO$_2$/SE│Li$_3$PS$_4$│Li$_{11}$Sn$_6$ cell measured after the sixth charging process. (e) Room-temperature cycling performance of the LiCoO$_2$/chloride-SE│Li$_3$PS$_4$│Li$_{11}$Sn$_6$ cell employing $Li_{2.633}Er_{0.633}Zr_{0.367}Cl_6$ as the chloride SE in the cathode composite. The cycling test was conducted at a current density of 0.55 mA cm^{-2} (3.0–4.3 V vs. Li/Li$^+$). Reproduced with permission.[58] Copyright 2020 ACS. (f) Crystal structures of Li_3YbCl_6-350 and $Li_{2.7}Yb_{0.7}Zr_{0.3}Cl_6$-350. (g) Structural evolution of Li_3YbCl_6–350 to $Li_{2.7}Yb_{0.7}Zr_{0.3}Cl_6$-350 upon Zr substitution. Li site and Tet site connectivity of (h) Li_3YbCl_6-350 along the [001] direction and (i) $Li_{2.7}Yb_{0.7}Zr_{0.3}Cl_6$-350 along the [100] direction. (j) Li$^+$ ion migration pathways in $Li_{2.7}Yb_{0.7}Zr_{0.3}Cl_6$-350. BVSE model of migration energy barriers for (k) Li_3YbCl_6-50 and (l) $Li_{2.7}Yb_{0.7}Zr_{0.3}Cl_6$-350. Reproduced with permission.[59] Copyright 2021 ACS.

SE for ASSLBs, which can be used as the benchmark for the novel halide-based SEs.

2.4. Hydroborate/Boro-Based Electrolytes

Hydroborate is an anion where hydrogen bonds with boron. The boron atoms can be substituted by carbon atoms and then produce carbonates.[78] Benefitting from the high hydrogen densities, hydroborate can be applied as a solid-state hydrogen storage device.[79] Besides hydrogen storage, hydroborate can also be used as a solid electrolyte for energy storage and conversion. Due to the specific structure and the electronic network, hydroborate-based solid-state electrolyte possesses some advantages, such as high thermal, chemical, and redox stability, low electronic and high ionic conductivities, and the appropriate mechanical properties (suitable hardness).[80] The relevant research concerning hydroborate-based electrolytes mainly focuses on the application of ion batteries (i.e., Na, Li, Zn), which involves the studies of crystal structure, mechanical properties, dendrite resistance, stability, and electrochemical properties.[81]

In the 1970s, the predecessor of hydroborate-based electrolytes, $Li_2B_{10}Cl_{10}$ and $Li_2B_{12}Cl_{12}$, were first applied as the electrolyte components.[82] Afterward, more and more research and efforts were invented to study the properties of hydroborate electrolytes. In 2007, Orimo et al.[83] first applied the HT hexagonal $LiBH_4$ as the electrolyte and found the strong ionic conductivity of $LiBH_4$. Subsequently, they continuously studied and improved the performance of $LiBH_4$. Through a series of experiments, they successfully stabilized the performance hexagonal phase $LiBH_4$ under room temperature and determined that the ionic conductivity of $LiBH_4$ is 10^{-4} S cm^{-1}.[84] Until now, the MBH_4, MB_3H_8, $M_2B_nH_n/MB_nH_n$ (n = 10, 12), $MCB_nH_{n+1}/MCB_nH_{n+1}$ (n = 9, 11), $MB_{11}H_{14}$, M-7-$CB_{10}H_{13}$, and M-7,8-$C_2B_9H_{12}$ (M═Li, Na, K, Mg, Ca, Ag) are the common members of the family of hydroborate-based electrolyte. According to the previous report, the ionic conductivity of hydroborate-based material can achieve 70 mS cm^{-1} at 300 K.[85]

As the emerging class of SEs, the history of hydroborate-based SEs is much shorter than the SE based on oxides, halides, and sulfides. Hydroborate-based SEs show remarkable SE properties in high-voltage batteries.[86] For example, the $Na_4B_{36}H_{34}$–7$Na_2B_{12}H_{12}$ is a high-voltage SE demonstrating high ionic conductivity of 1.02×10^{-3} S cm^{-1} and a wide electrochemical stability window of 5.5 V for all-solid-state sodium batteries. For ASSLBs, $LiCB_9H_{10}$ is the benchmark for hydroborate-based SEs, with an ionic conductivity of ~3.0×10^{-2} S cm^{-1} at 354 K.[85] On the other hand, novel nido-hydroborate-based SE for ASSLBs has been successfully prepared recently, with liquid-like room temperature ionic conductivity.[87] This new $Li_3(B_{11}H_{14})(CB_9H_{10})_2$ displays a remarkable ionic conductivity of 1.1×10^{-3} S cm^{-1} at 25 °C, which also is a cost-effective replacement of $LiCB_9H_{10}$.

2.5. Phosphide-Based SEs

Phosphide is a compound containing the anion P^{3-}, where these compounds can exist in wide structures, such as chain and cage form.[88] Most metals can bind with anion P^{3-} to form metal phosphide (MP) or transition metal phosphide (TMP).[89] On one hand, MPs/TMPs are commonly used as insecticides and rodenticides to protect grains and crops due to their high toxicity.[90] On the other hand, MPs/TMPs possess excellent electrocatalytic activity, low redox potential, high theoretical capacity of 2596 mAh g^{-1} (calculated from the formation of M_3P), high reserve abundance, and robust durability.[91] Owing to their excellent properties, MPs/TMPs are intensively applied to the field of electrochemistry, such as water splitting, fuel cells, batteries, energy conversion, and storage. However, the volume expansion and the low reaction kinetic during the cycle limit the applications of the phosphide-based electrolyte.

Due to the differences in structure, composition, and morphosis, the working principle of each phosphide-based electrolyte can be significantly different. Generally, the working principle mainly includes intercalation/deintercalation, chemical conversion, and alloying/dealloying mechanisms. The intercalation/deintercalation mechanism relates to the capacity generation of phosphide-based electrolytes, which involves the transportation of metal ions into or out of the phosphide-based electrolytes.[94] The chemical conversion mechanism commonly involves the enhancement of the storage performance of electrolytes. The M species evenly form and distribute within the MPs during the reaction of metal ions and phosphorus ions. Remarkably, the existence of M species enhances the electrochemical performance of the battery. Additionally, these species also prevent structural pulverization and accelerate electron transfer.[94] Finally, the alloying/dealloying mechanisms, affect the maximum performance of the electrochemical activity and the capacity of the battery.[95]

3. Organic Solid Electrolytes Classifications

Polymer (organic) SEs are being revisited as promising electrolytes for ASSLBs owing to their higher flexibility and processability. In particular, the polymer-based SEs can effectively suppress the growth of Li dendrite and avoid internal short circuits, which significantly increases the safety property of ASSLBs.[96] However, polymer-based SEs generally display lower room temperature ionic conductivity, low mechanical strength, limited electrochemical window, and weak thermodynamic stability compared to inorganic-based SEs.[97] The Li salt can fully dissolve in the polymer electrolytes to form the cation and anion, in which the Li$^+$ cation migrates via polymer chain movement. Therefore, the Li ionic conductivity of polymer-based SEs is determined by the number of free Li$^+$ cations as well as the moving ability of the polymer chain. Moreover, inorganic additives can be used as fillers to be compounded with polymer/Li salts, forming composite polymer electrolytes (CPEs). In general, inorganic fillers can improve the interface between the polymer electrolyte and the electrode and

Batteries & Supercaps

Review
doi.org/10.1002/batt.202400432

Chemistry Europe
European Chemical
Societies Publishing

enhance the interfacial compatibility between the polymer electrolyte and the Li electrode by capturing impurities in the battery system.[98] In the following part, we will briefly outline the common types of solid polymer SEs and polymer-based composite SEs for ASSLBs.

3.1. Solid Polymer Electrolytes (SPEs)

The Li salt utilized for SPEs requires low lattice energy, and the host polymer needs to possess a high dielectric constant to facilitate the dissociation and transport of ions.[99] Based on that, polymers with polar groups that can form coordination bonds with both anions and cations are chosen for constructing SPEs. In general, the lithium salt interacts with the polymer coordination sites to form the complex based on the acid-base theory, and the ion diffusion occurs in the presence of the propelling dynamic created from the motion of amorphous polymer chains, where the ion species dissociate, hop and coordinate repeatedly as the local segments regenerate at new adjacent coordination sites. The ion conductive process is a directional movement of ions driven by the external electric field. Therefore, ion transportation should occur in the amorphous phase, while the crystalline phase hinders ion migration.[100] For SPE materials, the ionic conductivity (σ) can be expressed as by:

$$\sigma = ne\mu$$

Where n, e, and μ are the effective number of mobile ions, the elementary electric charge, and the ion mobility, respectively. The common SPEs are dual-ion conductors, and both the cations and counter anions are movable in the amorphous region. This dual-ion transportation in SPEs causes the polarization issue, which limits the Li-supply toward the electrode and lowers the effective Li transference number due to the accumulation of counter anion on the anode site.[101] To address polarization issues, single-Li-ion SPEs were developed by fixing the anion to the polymer chain. The single-Li-ion SPEs have anions covalently bonded to polymers or immobilized by anion acceptors.[102] Consequently, the single-Li-ion SPEs show single-ion conduction with approximately unity Li-ion transference number.[103]

Polyethylene oxide (PEO) is the most used SPE for ASSLBs, and it possesses good chain flexibility, excellent electrochemical stability to Li metal, low glass transition temperature (T_g), and excellent solubility with Li salts.[104] The main issue of PEO-based SEs is poor ionic conductivity and low inferior Li-ion transference numbers (0.2–0.3) at room temperature due to the high crystallinity of PEO. Hence, the PEO-based SEs usually operate at high temperatures (above 60 °C).[105] On the other hand, several methods have been explored to address the crystallinity and low ionic conductivity of PEO. The ionic conductivity of PEO-based SEs performance can be enhanced via blending or copolymerization of the PEO with poly (methacrylic acid) (PMAA) to form a hydrogen bonding type inter-macromolecular complex matrix with dissolving LiClO$_4$ salt.[106] Furthermore, copolymerization can also improve Li-ion conductivity by

effectively reducing crystallinity and increasing the amorphous area for Li$^+$ transportation. Additionally, crosslinking is also an effective method to decrease crystalline domain. At the same time, crosslinking could also substantially improve the mechanical strength and thermal stability of the PEO-based-SPEs.[107] For example, polysiloxane has also been another candidate host for SPEs, in which the PEO-based-SPEs based on polysiloxane derivatives can have ion-conducting PEO side chains that crosslinked with modified gallic acid.[92] The crosslinked polymer (A-BPTPs) displayed a relatively high conductivity due to the highly flexible polysiloxane backbones, low glass-transition temperature (T_g), and excellent compatibility with Li metal anode (Figure 3a–f). It is also believed that the large number of crosslinking sites can increase the mobility of ion-conducting chains via crosslinking. Meanwhile, polymers with hyper-branched structures can effectively suppress crystallization. For example, Chen et al.[93] synthesized hyperstar polymers (hbPPEGMA$_m$-s-PS$_n$) using PEO and polystyrene (PS), in which the hyperbranched PEO served as the star core, and PS served as the arms. The hbPPEGMA$_m$-s-PS$_n$ displayed fast Li$^+$ transport (~0.1 mS cm^{-1} at 60 °C) due to the suppressed crystallization of the PEO domains. Meanwhile, the efficient entanglement of linear PS arms during phase separation also improved the mechanical property, leading to a high Li/SPE interface stability without lithium dendrite growth (Figure 3g–m).

3.2. Composite Polymer Electrolytes (CPEs)

Instead of using blending, copolymerization, crosslinking, and hyperbranched structure, the performance of SPEs can also be enhanced by adding various types of filler additives to form composite polymer electrolytes (CPEs).[108] The CPEs mainly consist of host polymers, Li salts, and inorganic additives (fillers), and the inorganic fillers play a key role in comprehensive performance. Recently, the CPEs have exhibited excellent electrochemical and safety properties. The CPEs can gain the advantage from each of their respective components, enhancing their properties, including ionic conductivity, mechanical properties, interfacial stability, and electrochemical windows.[109] For example, adding inorganic filler can improve the interface between the polymer electrolyte and the electrode while enhancing the interfacial compatibility between the polymer electrolyte and the lithium electrode by capturing impurities in the battery system. However, the practical application of CPEs is still limited by their relatively low ionic conductivity of the electrolyte and high interfacial impedance. Therefore, solving the ionic conductivity and interfacial issues are the two key focus areas for the research in CPEs. Depending on the influence of the filler on the ionic conductivity, the inorganic fillers can be divided into passive and active fillers.

For passive fillers, although the ionic conductivity of CPEs can be increased by incorporating passive fillers, the passive fillers themselves do not possess ion transport capabilities (lithium-ion insulators). The improvement of ionic conductivity by incorporating passive filler depends on the filler-polymer interface, where the passive fillers can affect the ion transport
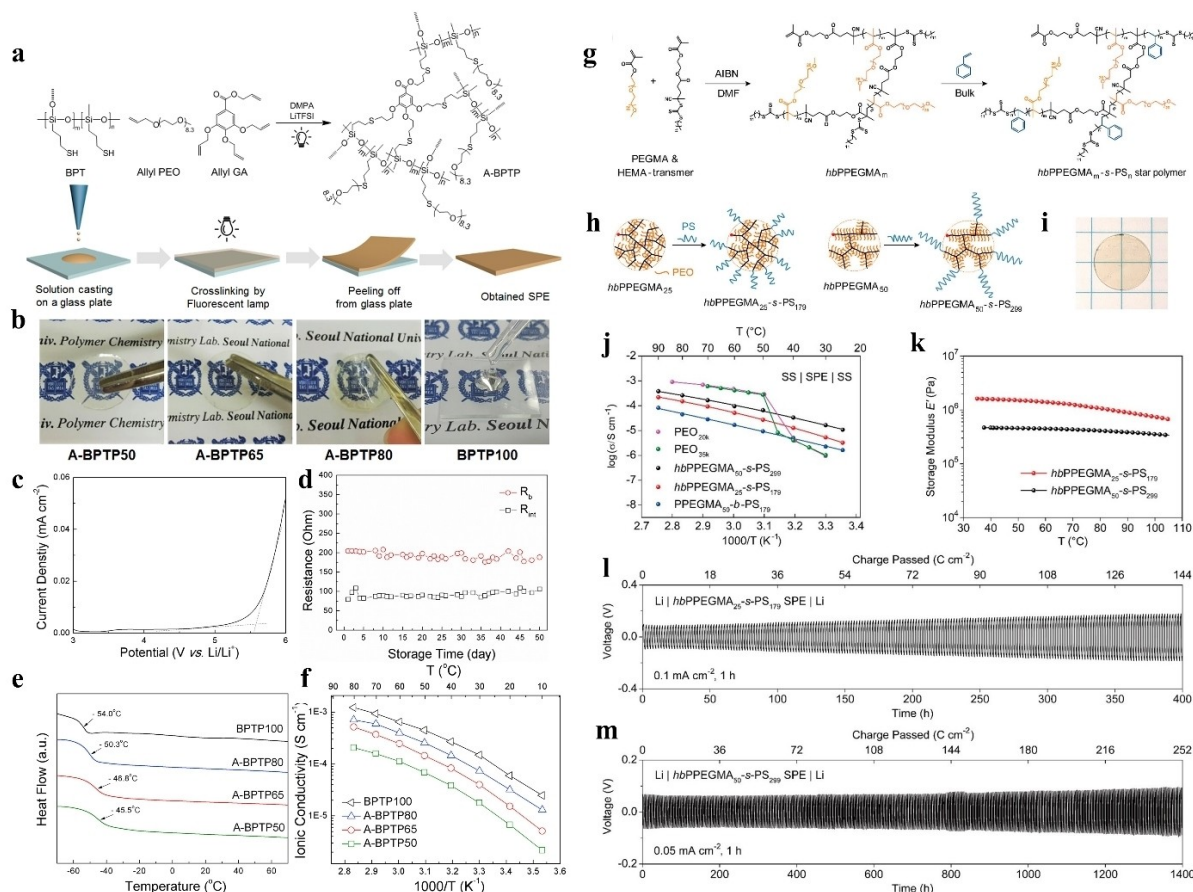
Batteries & Supercaps

Review
doi.org/10.1002/batt.202400432

Chemistry
Europe
European Chemical
Societies Publishing

Figure 3. (a) Preparation of A-BPTPs crosslinked polymer and (b) photographs of A-BPTPs having free-standing film states and BPTP100 having a wax state, where the number in the name indicates mol% of allyl PEO. (c) Linear sweep voltammogram A-BPTP80 at 60 °C with a scan rate of 1 mV s^{-1} and (d) bulk resistance (R_b) and interfacial resistance (R_{int}) of symmetric Li/A-BPTP80/Li cell stored under open-circuit condition at 60 °C as a function of storage time. (e) DSC thermograms and (f) temperature dependence of ionic conductivities of BPTP100 and A-BPTPs ([Li]/[EO] = 0.07). Reproduced with permission.[92] Copyright 2017 Elsevier. (g) Synthetic route of *hb*PPEGMA$_m$-s-PSn hyperstar polymers. (h) Schematic of hyperbranched *hb*PPEGMA$_m$ and *hb*PPEGMA$_m$-s-PS$_n$ polymers with different average chain lengths of branched PEO and linear PS. (i) Digital photograph of hbPPEGMA$_{50}$-s-PS$_{299}$ SPE membrane. (j) Temperature-dependent ionic conductivity. (k) Storage modulus E'. Li plating/stripping voltage profiles versus cycle time and charge passed of Li|*hb*PPEGMA$_m$-s-PS$_n$ SPE|Li symmetric cells cycled at 60 °C with 1 h charge and 1 h discharge at a current density of (l) 0.1 mA cm^{-2} for *hb*PPEGMA$_{25}$-s-PS$_{179}$ SPE and (m) 0.05 mA cm^{-2} for *hb*PPEGMA$_{50}$-s-PS$_{299}$ SPE. Reproduced with permission.[93] Copyright 2019 ACS.

capability of polymer chain segments.[110] For instance, adding passive fillers (such as plasticizers or ceramics) can improve ion transport efficiency by suppressing polymer crystallization (increasing the amorphous phase).[111] In addition, passive fillers can support the polymer matrix and increase the mechanical strength, while the surface of passive fillers would interact with ion pairs to promote further dissociation based on Lewis acid-base theory. Common passive fillers such as Al$_2$O$_3$,[115] Fe$_2$O$_3$,[116] TiO$_2$,[117] and SiO$_2$,[118] are widely used to increase the ionic conductivity of CPEs due to their controllable size and high stability.

In contrast to the passive fillers, the active fillers not only can reduce the crystallinity of the polymer matrix but also contain continuous ion channels in the bulk phase that can facilitate ion transport.[119] Hence, it is believed that the active fillers based on lithium fast-ion conductors that possess high ion conductivity can improve the ionic conductivity of CPEs more effectively. The high ionic conductivity active fillers usually

have numerous continuous defects with low activation energy, allowing easy ion hopping.[120] Meanwhile, active fillers can also serve as a Li$^+$ source that increases the movable Li$^+$ at the filler-polymer interface. Perovskite, garnet, and LISICON are inorganic materials that are commonly used as the active filler for CPEs, while NASICON-type electrolytes like LAGP and LATP were also can be used as an effective active filler to improve both ionic conductivity and stability of PEO-based SEPs.[121] Recently, the most used active fillers are different kinds of lithium salts, such as LiTFSI and LiClO$_4$.[122] The additional lithium salt can increase ionic conductivity via a direct increase in the number of charge carriers. Besides, ionic liquids such as [1-ethyl-3-methylimidazolium bis(trifluoromethylsulfonyl)imide, (EMIM)(TFSI),[123] and 1-butyl-3-methylimidazolium chloride,[124] are also drawing tremendous attention because of their ability to reduce the crystallinity, which indirectly increases the conduction.

Although the PEO is considered the unrivaled benchmark for the SPE for battery application, the pure PEO without further modification or filler additive is not considered the benchmark owing to its poor ionic conductivity and narrow electrochemical window (> 3.6 V). Based on that, the high-performance organic-based SEs usually have passive or active fillers. The PEO-LiTFSI (LiTFSI = lithium bis(trifluoromethanesulfonyl)imide) SE are commonly used as starting points in designing next-generation polymer electrolytes. The PEO-LiTFSI exhibited a high ionic conductivity of 1.5×10^{-5} S cm^{-1} at 25 °C, which is considered as the benchmark for SPE.[125] For all the different solid electrolytes, we have supplied a comparison Table to demonstrate the representative materials, ionic conductivity, main advantages, and drawbacks of different SEs (Table 1).

4. Recent Advances of Solid Electrolytes

4.1. Inorganic Electrolyte

4.1.1. Sulfide-Based SEs

Even though the sulfide-based electrolyte is famous for the lithium battery, the development of this electrolyte is still ongoing. Hong et al.[126] developed a thin, high flexibility, high ionic conductivity, and high mechanical strength sulfide-based electrolyte. They combined the EMG terpolymer (polyethylene-co-methyl acrylate-co-glycidyl methacrylate with the Li$_6$PS$_5$Cl (argyrodite) to obtain the solid electrolyte. At 60 °C, the solid electrolyte showed satisfactory interfacial stability with Li and a high ionic conductivity of 1.88 mS cm^{-1}. Moreover, they combined the Li–In anode, EMG-based solid electrolyte sheet, and the LiNi$_{0.9}$Co$_{0.05}$Mn$_{0.05}$O$_2$ cathode to produce the whole solid-state cell. At 0.05 °C and 60 °C, the cell possesses a discharge capacity of 229.2 mAh g$^-$, which is equal to the areal capacity of 5.5 mAh cm^{-1}.

Besides the interfacial stability and ionic conductivity, they also improved the energy density of sulfide-based electrolytes.[112] The idea of improving the energy density of sulfide-based electrolytes is that enhance the loading of active material in the composite cathode. The composite cathode consists of the LiNi$_x$Co$_y$Mn$_{1-x-y}$O$_2$ (NCM) materials and Ni. The content of Ni (70 and 82%) particle size (4, 5, and 10 μm) and the crystallization form (single and polyform) are variables to determine the suitable conditions for optimizing the performance of electrolytes. Figure 4a–c shows the structure of the single crystal, small polycrystalline, and large polycrystalline NCM. The experimental result shows that the single crystalline LiNi$_{0.82}$Co$_{0.1}$Mn$_{0.08}$O$_2$ with SNi82-5 and small particle size exhibit the best performance. The product exhibits a high discharge capacity of 193.2 mAh g^{-1} and an active mass loading of 26 mg cm^{-2} (equal to the areal capacity of 5.0 mAh cm^{-2}).

In addition to the actual performance, the stability of the sulfide-based SEs at the ambient condition is another factor that needs to be considered during the operation. To enhance the moisture stability of the sulfide-based SE, Jin et al.[127] fluorinate the Li$_{10}$GeP$_2$S$_{12}$ to form the LiF-coated core-shell solid electrolyte LiF@Li$_{10}$GeP$_2$S$_{12}$. In 30% relative humidity air, the SE exhibits excellent moisture stability. They applied the DFT to determine the hydrolysis mechanism of the Li$_{10}$GeP$_2$S$_{12}$, which brings the moisture stability of the product. After exposure to the air for 40 min, the ionic conductivity of the LiF-coated core-shell SE is 1.46×10^{-3} S cm^{-1}. Besides the LiF-coated core-shell SE, they combined the LiNbO$_3$@LiCoO$_2$, LiF@Li$_{10}$GeP$_2$S$_{12}$, and Li to assemble the battery. The initial discharge capacity and the capacity retention of the assembly battery are 101.0 mAh g^{-1} and 94.8% after 1000 cycles at 1 °C, respectively.

Zhang et al.[128] study the Li$_{10}$GeP$_2$S$_{12}$ and applied the stannous fluoride doping method to synthesize the fluorine functionalized Li$_{10}$GeP$_2$S$_{12}$ and used the product as the stable monolayer solid electrolyte. They used the DFT calculation to study the atomic-scale mechanism, which involves the moisture

Table 1. The Summary of SEs for ASSLBs with their main advantages and drawbacks.

| Type	Example	Ionic Conductivity at 25 °C (S cm^{-1})	Advantages	Drawbacks
Oxide SEs	LISICON (LiGe$_x$Ti$_{2-x}$(PO$_4$)$_3$) LLTO (La$_{2/3-x}$Li$_{3x}$TiO$_3$) LLZO (Li$_7$La$_3$Zr$_2$O$_{12}$)	10^{-3} to 10^{-4}	High ionic conductivity Excellent chemical & electrochemical stability	Non-flexible & brittleness Poor physical contact with electrode
Sulfide SEs	Li$_2$S-P$_2$S$_5$ Li$_2$S-MS$_2$	10^{-2} to 10^{-3}	High ionic conductivity High flexibility Low grain-boundary resistance	Poor air stability Low interfacial compatibility with cathode
Halide SEs	Metal halide: Li$_3$MX$_6$ (M=Y, Er, Yb, X=F, Cl, Br, I)	10^{-3} to 10^{-4}	Good compatibility with Li Widest electrochemical window (F-based SEs)	Poor air stability (Cl$^-$ & Br-based SEs) Low ionic conductivity (F-based SEs)
Hydroborate SEs	LiBH$_4$ Li$_2$B$_{12}$H$_{12}$-Al$_2$O$_3$	10^{-3} to 10^{-5}	Excellent redox stability with Li electrode	Low interface stability with high-voltage cathodes
Phosphide SEs	Li$_8$TtP$_4$ and Li$_9$TrP$_4$ (Tt=Si, Ge, Sn; Tr=Al, Ga)	10^{-2} to 10^{-4}	High ionic conductivity Low redox potential Robust durability	Relatively low conductivity
Organic SEs	PEO	10^{-5} to 10^{-7} 10^{-3} to 10^{-4} (with filler)	Good compatibility with Li High flexibility	Poor ionic conductivity (no fillers) Low thermal stability Limited electrochemical window
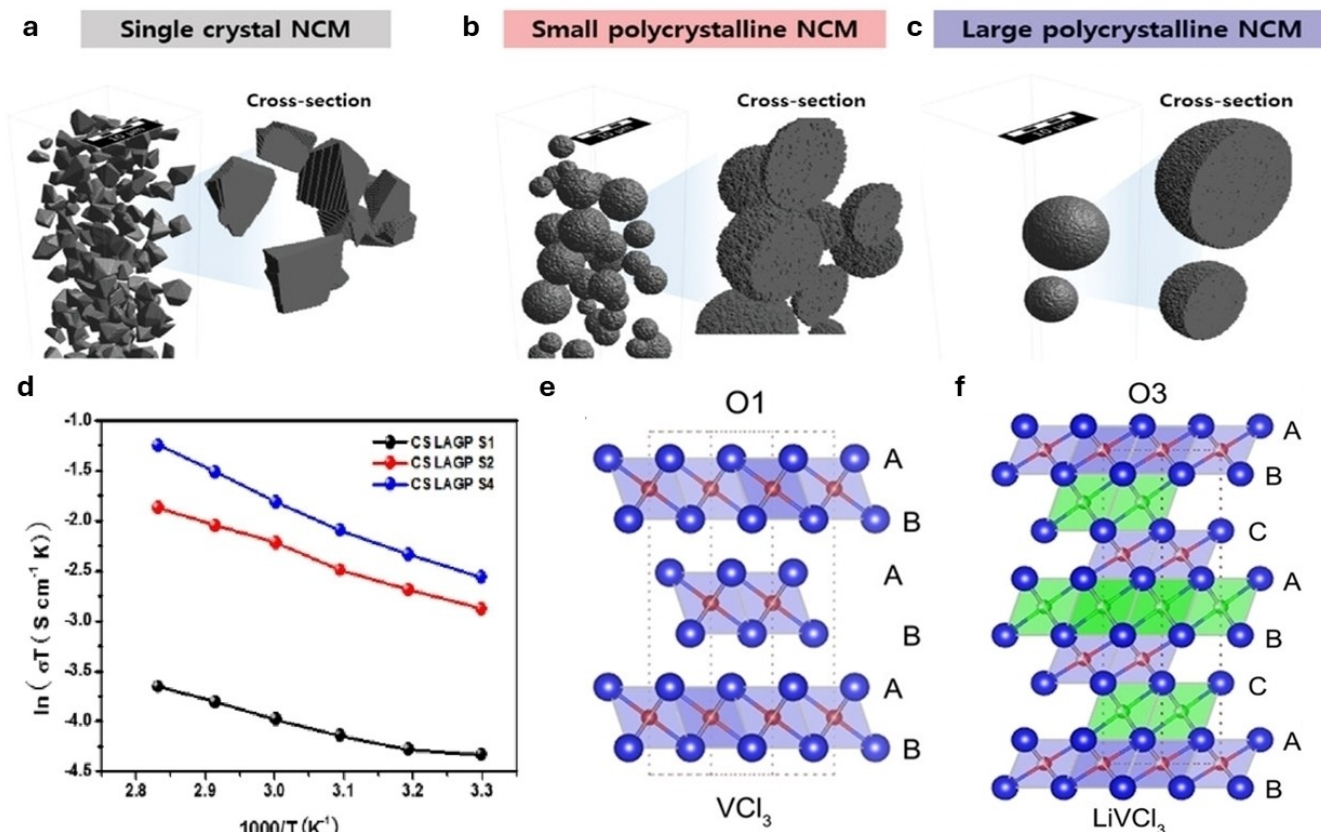
Figure 4. The structure of (a) single crystal, (b) small polycrystalline, and (c) large polycrystalline of NCM. Reproduce with permission[112] Copyright 2023 Wiley (d) The plot of conductivity versus temperature of sample. Reproduce with permission.[113] Copyright 2024 Elsevier. The crystal structure of (e) VCl_3 and (f) $LiVCl_3$ (the layered O1 structure). Reproduced with permission.[114] Copyright 2023 Wiley.

and electrochemical stability of the fluorine functionalized $Li_{10}GeP_2S_{12}$. Through the DFT calculation, they discovered that the retardation of the hydrolysis reaction of $Li_{10}GeP_2S_{12}$ caused by the electronic regulation, which is contributed to the reduction of surface hydrophilicity from the fluorine surface doping. Under relative humidity of 35%–40% and exposure for 20 min, the ionic conductivity of the SE is 2.21 mS cm^{-1}. Benefitting from the doping of fluorine, the ASSLB assembled by fluorine functionalized $Li_{10}GeP_2S_{12}$ exhibits the critical current density of 2.1 mA cm^{-2} and 80.1% retention after 600 cycles at 1 °C.

4.1.2. Oxide-Based SEs

The oxide-based solid electrolyte is commonly used for lithium batteries and has attracted the attention of researchers recently due to its structural stability and other excellent properties. Nevertheless, more and more efforts have been made to further improve the performance and explore the application of these materials. Ahmad et al.[129] employed the conventional method to synthesize the novel oxide-based ternary composite ($AlPO_4$-$SiOLi_4P_2O_7$) electrolyte, where the product exhibits high water stability and ionic conductivity. Through the analysis of the x-ray diffraction, they determined the crystallographic structure

of the ternary composite and thus found that the ionic conductivity is significantly influenced by the structure. Besides, they also applied electrochemical impedance spectroscopy to determine the ionic conductivity of the electrolytes. At ambient temperature, the ionic conductivity of the Mn-ternary composite is 1.63×10^{-6} S/cm, where it can enhance up to 1.68×10^{-6} S/cm by applying 8 wt%-LiBr for reducing the grain boundaries.

The side reaction and lithium loss from the high-temperature sintering (HTS) process limits the application of oxide solid electrolyte (OSE). To overcome these limitations, Sun et al.[113] designed a near-room-temperature (60 °C) cold sintering process to produce the OSE. This process applied a low-melting-point plastic crystal electrolyte (PCE) to fill the grain boundaries (GBs). Under the ambient temperature, the ionic conductivity and transference number of electrolytes reached up to 0.25 mS cm^{-1} and 0.88, respectively. Figure 4d shows the relationship between the conductivity and temperature. At a current density of 0.1 mA cm^{-2}, the cell can operate for 2000 h, which exhibits the ability of electrolytes to suppress side reactions and maintain the interfacial stability of the cell. After 820 cycles (566 days) at 0.1 °C rate, the capacity retention of the full cell is around 70%.

Batteries & Supercaps

Review

doi.org/10.1002/batt.202400432

Chemistry
Europe
European Chemical
Societies Publishing

4.1.3. Halide-Based SEs

Although the halide-based solid electrolyte is intensively applied for the lithium battery due to its excellent performance, the study of these materials is actively ongoing. Liang et al.[114] reported a novel V^{3+}/V^{2+} chloride cathode in the halide-based solid-state electrolyte for the lithium battery. The cell exhibits high interfacial stability and the VCl_3 cathode enables the high reversible redox reaction, owing to the chemical stability between the VCl_3 cathode and halide electrolyte. Figure 4e and f show the crystal structures of VCl_3 and $LiVCl_3$. Moreover, the all-solid-state battery demonstrates satisfactory performance, including high reversible capacity, high rate, and long-life cycle (85% capacity retention, 6°C, over 200 cycles). Further, under extreme temperatures and ultra-high loading, the battery still exhibits good performance.

Kwak et al.[130] developed a halide nanocomposite solid electrolytes (HNSEs) $ZrO_2(-ACl)$-A_2ZrCl_6 (A=Li or Na) to improve the electrochemical performance of the lithium and sodium batteries. At 30°C, compared to the A_2ZrCl_6, HNSE enhances the ionic conductivity of Li and Na batteries from 0.40 to 1.3 mS cm^{-1} and from 0.011 to 0.11 mS cm^{-1}, respectively. Moreover, they developed the fluorinated ZrO_2–$2Li_2ZrCl_5F$ HNSE, which exhibits high-voltage stability and interfacial compatibility with Li_6PS_5Cl. Furthermore, they assemble the ASS lab-scale cell, Li–In || $LiNi_{0.88}Co_{0.11}Mn_{0.01}O_2$. Under the testing at

the temperature of 30°C and pressure of 70 MPa, the cell demonstrates the specific discharge of 115 mAh g^{-1} after almost 2000 cycles at 400 mA g^{-1}.

4.1.4. Hydroborate-Based SEs

Sakamoto et al.[131] combined two materials, including the conductive $Li_7La_3Zr_2O_{12}$ (LLZ) and sintering-free $LiBH_4$, to create a composite-based electrolyte. The composited LLZ-$LiBH_4$ was synthesized by mixing LLZ powder with $LiBH_4$, where the mixing ratio depends on the mass and density. LLZ powder was produced by hand milling and ball milling at room temperature. In this case, the hand milling method produced the LLZ-$LiBH_4$ composite with higher density, because of the more intensive particle size distribution of LLZ powder. Moreover, after hand milling, the composite electrolyte did not exhibit the formation of a secondary phase. When the volume ratio of LLZ increases to 0.8, the total ion conductivity of the whole composite increases with the increase of the LLZ ratio, because of the filling of $LiBH_4$ between the interspace of LLZ particles. Under room temperature, the optimized composite exhibited ionic conductivity of 5.8×10^{-5} S cm^{-1}, which is 670 times higher than that of $LiBH_4$ alone. Figure 5a, b shows the ionic conductivity of the product at different conditions. Figure 5c shows the nominal volume fraction of LLZ. At around 120°C, $LiBH_4$
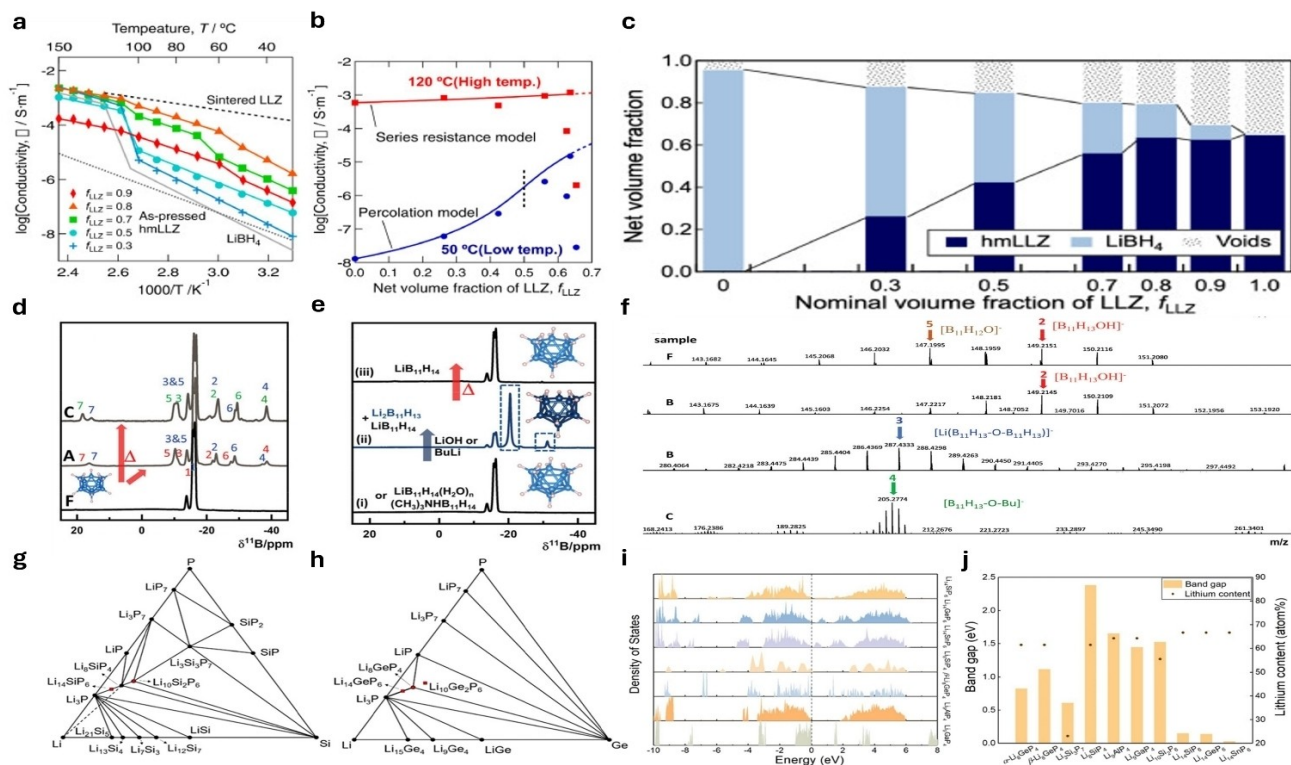

Figure 5. (a)The ionic conductivity of different hand milling LLZ-$LiBH_4$ composites (b)The ionic conductivity at 50°C and 120°C versus the net volume fraction of LLZ. (c) The plot of the net volume fraction versus the nominal volume fraction of different LLZ product. Reproduced with permission.[131] Copyright 2023 Elsevier. The ^{11}B (^1H) NMR spectra of (d) $LiB_{11}H_{14}(H_2O)_n$ and $LiB_{11}H_{13}R$ after heat treatment under different conditions, and (e) (i) the precursors $(CH_3)_3NHB_{11}H_{14}$ or $LiB_{11}H_{14}(H_2O)_n$, (ii) the mixture of $LiB_{11}H_{14}$ and $Li_2B_{11}H_{13}$ in basic solutions, and (iii) of pure $LiB_{11}H_{14}$ after heat treatment. (f) The ESI-MS with $^{11}B/^{10}B$ isotopic patterns assigned to 2–5 for different samples. Reproduced with permission.[132] Copyright 2021 Wiley. The phase diagrams of (g) Li-Si–P and (h) Li-Ge–P. The (i) density of state and (j) band gap of the solid electrolytes. Reproduced with permission.[133] Copyright 2022 ACS.

Batteries & Supercaps

Review
doi.org/10.1002/batt.202400432

Chemistry Europe
European Chemical
Societies Publishing

undergoes a phase transition to high temperature conduction phase. Under such a conduction phase, the Li-ion conduction behavior changed from a percolation model to a series resistance model. Furthermore, the composite formed an interface to Li metal, where the voltage endurance is 0.5 mA cm^{-2} at 100 °C.

Payandeh et al.[132] reported the use of nido-hydroborate (lithium tetradecahydroundecaborate, LiB11H14) to replace the LiCB$_9$H$_{10}$. First, they applied the n-butyllithium (LiC$_4$H$_9$, BuLi), (CH$_3$)$_3$NHB$_{11}$H$_{14,}$ and tetrahydrofuran (THF) solution to synthesize the LiB$_{11}$H$_{14}$. After the synthesis, they used the ^{11}B nuclear magnetic resonance spectroscopy (NMR) and electrospray ionization high-resolution mass spectrometry (ESI-MS) to identify the impurities and then eliminate them (Figure 5d–f). Closo-hydroborates and carba-closo-hydroborates are used for the following synthesis process. They obtained the Li$_2$(B$_{11}$H$_{14}$)(CB$_{11}$H$_{12}$) and the Li$_3$(B$_{11}$H$_{14}$)(CB$_9$H$_{10}$)$_2$ with the ionic conductivity of 1.1×10^{-4} S cm^{-1} and 1.1×10^{-3} S cm^{-1}, respectively. Moreover, through the Density Functional Theory (DFT) calculations, they determined the oxidative stability of LiB$_{11}$H$_{14}$ is 2.6 V versus Li$^+$/Li. Furthermore, they combined the Li$_2$(B$_{11}$H$_{14}$)(CB$_{11}$H$_{12}$) electrolyte with the TiS$_2$ cathode to produce a proof-of-concept half-cell, where the capacity retention is 82% after 150 cycles at C/5.

4.1.5. Phosphide-Based SEs

Maltsev et al.[134] combined first principle calculation and machine learning to investigate the ionic conductivity of the lithium phosphide. For the first principle DFT calculation, the Vienna Ab initio Simulation Package (VASP), projector augmented-wave method with plane-wave basis set, and the Perdew-Burke-Ernzerhof (PBE) exchange-correlation functional were selected as the parameter. For machine learning, Ab Initio Molecular Dynamics (AIMD) was selected to collect the dataset of the machine learning interatomic potential (MLIP). Through the combination, they calculated the convex hull of the lithium phosphide product at different temperatures and then obtained a temperature-composition phase diagram. The lithium phosphide can be classified as stable (Li$_3$P, LiP, Li$_3$P$_7$, Li$_3$P$_{11}$, LiP$_7$) and metastable (Li$_4$P$_3$, Li$_5$P$_4$, LiP$_5$) compound, where the ionic conductivity of these compounds was investigated as the function of temperature. In addition, Li$_3$P, LiP$_5$, Li$_5$P$_4$, Li$_4$P$_3$, and Li$_3$P$_7$ appeared high lithium diffusion, with ion conductivity in the range of 10^{-4}–10^{-2} S cm^{-1} at room temperature. In the temperature range of 300–500 °C, the lithium diffusion did not happen in the LiP, Li$_3$P$_1$, and LiP$_7$, where the ion conductivity of these lithium phosphides was the lowest. Moreover, they observed a different relationship between the ion conductivity and the arrangement of phosphorus atoms. In the case, of the 3D network arrangement lithium phosphides possess 1D conductivity, the chains and broken chains of lithium phosphides exhibit 2D conductivity, whereas the lithium phosphides with other structures result in 3D conductivity. The team of Min reported their study concerning the lithium-rich ternary phosphide through the first principle calculation.[133] Through the first-principles DFT calculations and the thermodynamic

analysis, they investigated the phase stability, electrochemical stability, and the phase equilibrium of 10 lithium-based phosphide types of SE. First of all, they constructed the phase diagrams at 0 K. The results from the phase diagrams explain the availability for synthesizing lithium-based phosphides composite and indicate that the stable phase results from the bonding of phosphorus with other atoms. To determine the electrochemical stability, they calculated the Density-of-State (DOS) and the band gap of the SE (Figure 5g–j). These results show that the electrochemical stability of the SEs is narrower than 0.5 V. The various P binary compounds form from the oxidation of SE, causing the lower anodic limits of about 1 V vs Li/Li$^+$. However, the lower anodic limit implies that the SE possesses poor cathodic electrochemical stability. Besides the phase and electrochemical stability, they discovered that the new phases formed at the interface are the critical factors for the thermodynamic driving force of these SEs. Moreover, through the analysis of the Li diffusion kinetics, the face-sharing octahedral and tetrahedral sites possess a low energy barrier, leading to the high efficiency of Li conduction.

4.2. Organic Solid Polymer Electrolytes

Although solid polymer is one of the common organic electrolytes for the lithium battery, the problems of ionic conductivity and mechanical strength still need to be overcome for better performance. To overcome these problems, Zang et al.[135] developed a local high-concentration solid polymer electrolyte for the lithium battery. The design of the electrolyte is based on the polymer blends, which it named Li-polymer in F diluter (LPIFD). The combination of lithium and polymer ensures continuous Li$^+$ conduction channels and benefits the solid electrolyte interphase (SEI). Besides, the F diluter enhances the mechanical strength of the electrolyte. The ionic conductivity of LPIFD is 3.0×10^{-4} S cm^{-1}, and the Coulombic efficiency and critical current density of Li anode achieved 99.1% and 3.7 mA cm^{-2}, respectively (Figure 6a). Moreover, the formation of F-rich cathode electrolyte interphase brings the satisfactory performance of the lithium battery, where the battery can work 450 cycles at an operating voltage of 4.5 V (Figure 6b and c).

Besides the actual performance, the stability of the electrolyte is also essential for the battery during the operation. Peng et al.[136] improved the stability and the ionic conductivity of the solid polymer electrolyte. They developed a novel solid polymer electrolyte, which is termed fluorinated backbone and oligomer batteries in terms of columbic efficiency, cycle lifetime, and capacity retention (Figure 6d and e). Moreover, they produced a 2.6 Ah pouch cell containing the graphite anode, PFVS electrolyte, and the NCM90 cathode, which exhibits stable cycling and application potential.

4.3. Composite Electrolytes

The application of poly (ethylene oxide) (PEO) and the garnet-type material Li$_{6.4}$La$_3$Zr$_{1.4}$Ta$_{0.6}$O$_{12}$ (LLZTO)-based composite elec-
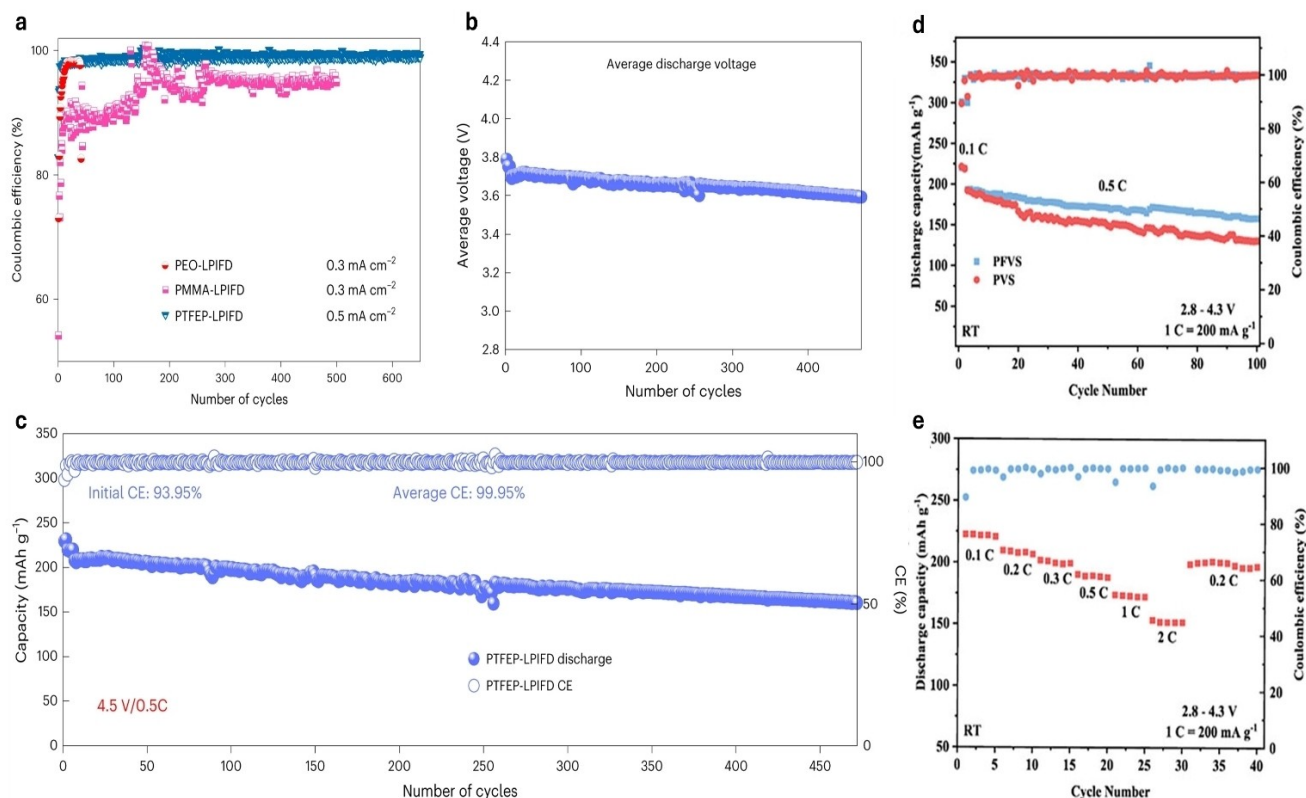
Figure 6. (a) The Coulombic efficiency of different LPIFD with polymer products under different cycling. (b) The average discharge voltage and the (c) cycling performance of the coin cells with NMC811 cathodes at 4.5 V cutoff voltage using PTFEP-LPIFD. Reproduced with permission.[135] Copyright 2024 Nature. (d) The Cycling performances of Li||NCM811 cells at 0.5 °C rate with different electrolytes. (e) Rate performance of Li /PFVS/NCM811 cells. Reproduced with permission.[136] Copyright 2024 Wiley.

trolyte is limited by the ionic conductivity and the interfacial resistance. The team of Khan reported the novel designed composite electrolyte for improving the electrochemical performance of the lithium battery.[137] They combined active and inactive fillers to invent a hybrid filler-designed solid polymer electrolyte and applied it to enhance the properties of both the lithium metal anode and the LiFePO₄ cathode. They applied scanning electron microscopy (SEM) to observe the surface of Li at different periods. (Figure 7a–d) The novel electrolyte ensures the interfacial stability and the cycling performance for 2000 h at a current density of 0.1 mA cm^{-2} and stabilizes the cycling of LiFePO₄//Li full battery for 400 cycles at 1 °C. Moreover, at 40 °C, the maximum ionic conductivity and the Li$^+$ transference number of these batteries with the novel electrolytes can reach 1.9×10^{-4} S cm^{-1} and 0.67, respectively. These satisfactory results contribute to the strong affinity to Li$^+$ and low interfacial resistance of hybrid fillers.

Fan et al.[138] developed an air-processable technique to synthesize the solid composite electrolyte and avoid the undesired reaction from ambient moisture. The technique combined the $LiCF_3SO_3$ (LiOTf) (Li salt), $Li_{6.4}La_3Zr_{1.4}Ta_{0.6}O_{12}$ (LLZTO) (fast Li-conductor), and the polyvinylidene difluoro ethylene/polyvinyl acetate (PVDF/PVAC) (polymer matrix). The trace amount of H_2O in the electrolyte solution significantly enhances the Li$^+$ conductivity of solid composite electrolytes to

5.09×10^{-4} S cm^{-1} at room temperature. The oxygen H_2O tends to interact with the Li atom in LiOTf, therefore, forming the hydrogen bond with the oxygen atom in the solvent. LiOTf dissociates due to such interaction, and results in the formation of uniform Li$^+$ transportation channels. At 0.2 °C, the initial Coulombic efficiency and capacity retention rate of the battery are 94.7 % and 96 % after 180 cycles, respectively. At 0.5 °C, the capacity of the battery is 143.7 mAh g^{-1} after 150 cycles (Figure 7e and f). Song et al.[139] employed the niobium-based Li-rich disordered rock salt (DRS) to form the shell on the surface of carbon material (Nb-DRS). They applied the shelled carbon material to perform efficient Li protection, which benefits the Li$^+$ diffusion network for accelerating carbon lithiation. The Li anode is protected by the Nb-DRS, where the protection brings the extra-stable cycling over 7000 cycles at high charge/discharge rates of 3 C/3 C. In addition, the improved ASSLB possesses a capacity of 3 mAh cm^{-2} and a relatively low negative/positive ratio of 5. Based on the detailed analysis of the performances, we have supplied a performance comparison Table 2 of different types of recent advanced solid electrolytes.
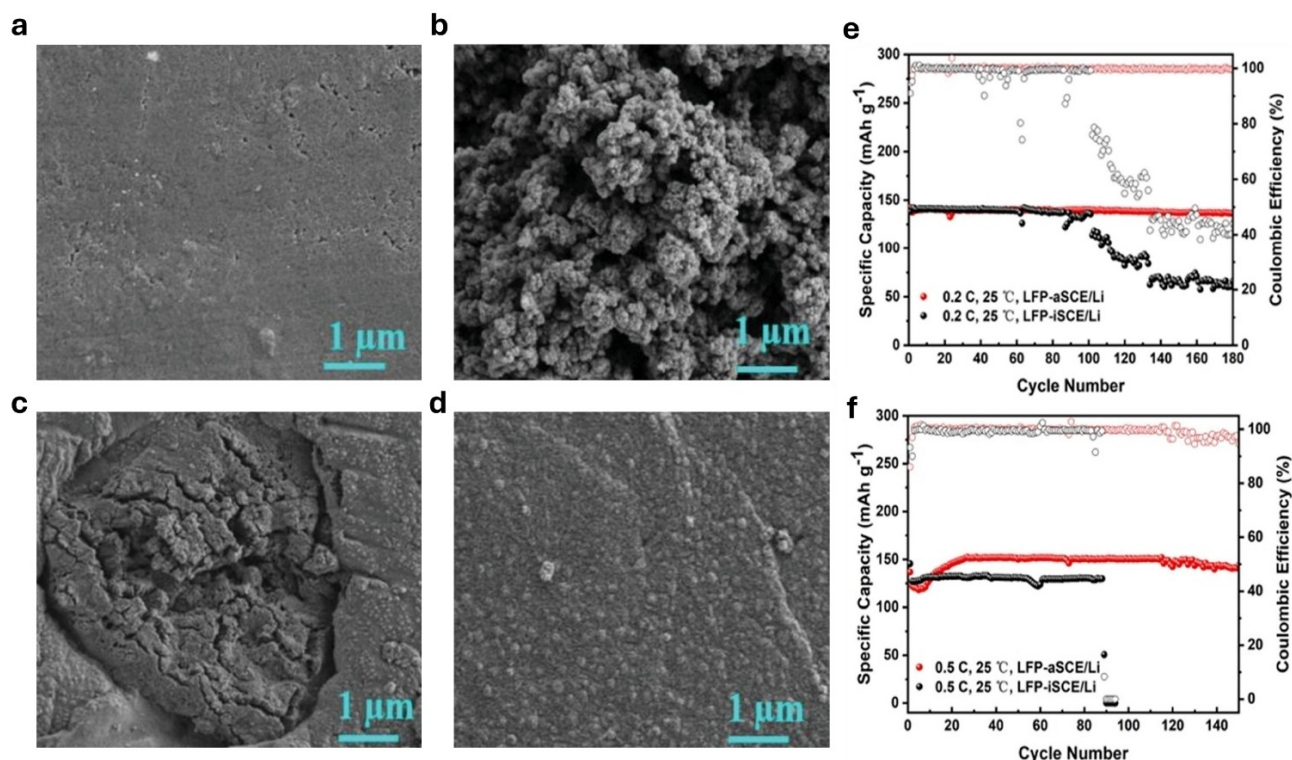
Batteries & Supercaps

Review
doi.org/10.1002/batt.202400432

Chemistry Europe
European Chemical
Societies Publishing

Figure 7. The SEM image of Li (a) before the work cycling, (b) after cycling with PL electrolyte membrane, (c) after cycling with PL-10 L electrolyte membrane, (d) after cycling with PL-10 L (L@3 W) electrolyte membrane. Reproduced with permission.[137] Copyright 2023 Wiley. The cycling performance of the LFP-aSCE/Li and LFP-iSCE/Li batteries (e) at 0.2 °C under 25 °C, (f) at 0.5 °C under 25 °C. Reproduced with permission.[138] Copyright 2024 ACS.

5. Synthesis Method of Solid Electrolytes

Synthesis is a critical process for all chemicals, which directly influence the yield, properties, structure, and performance of the product. Additionally, the complexity, mechanism, and cost, are the factors that require to be considered before the synthesis of chemical products. For instance, flow processing and batch production are the possible patterns to produce the chemical on a large scale. Compared to the batch method, the flow process benefits chemical manufacturing, including higher control temperature and pressure, smaller operation volume, more safety intermediates, and less production time.[140] In contrast, traditional batch production provides a high flexibility, low cost, and better-quality control approach to manufacturing chemicals. The safety issue, efficiency, technique, related personnel, time consumption, resources, working area, and other factors, are necessary to consider before the production of solid electrolyte. In this part, the synthesis methods of SEs will be classified into 4 types: inorganic electrolyte synthesis, solid polymer/composite electrolyte synthesis, direct writing-based 3D printing, and lithography-based 3D printing.

5.1. Inorganic Electrolyte Synthesis

Inorganic electrolytes are the common types of electrolytes used in lithium batteries. Benefitting from the flammable and withstanding higher temperatures, inorganic solid electrolyte opens the limited windows from liquid electrolytes. The efforts invested by scientists facilitate the development of solid electrolytes toward better ion conductivity, electrochemical stability, and mechanical properties. The synthesis process would significantly influence the performance, in terms of morphology, purity, phase, crystallinity, and other characteristics. The selection of synthesis would change the properties of materials, even for those with the same precursors. As a result, the synthesis method should be considered carefully before production for the yield and performance of products.

5.1.1. Sol-Gel Method

Sol-gel method is a wet chemical technique that is commonly applied to synthesize different organic and inorganic materials, such as electrolytes, fiber wood, and ceramic. In 1931, Kistler synthesized the aerogel, which may be the first sol-gel product.[141] After that, in the late 1960s to early 1980s, the sol-gel technology was gradually developed and explored applications. For instance, Roy heated the gelled water glass to synthesize small silica glass pieces in 1969.[142] In 1981, the first sol-gel workshop was held in Padova, Italy, where 80 participants from 8 countries joined in this workshop.[143] This workshop is an important milestone throughout the development of the sol-gel method.

Batteries & Supercaps

Review
doi.org/10.1002/batt.202400432

Chemistry Europe
European Chemical
Societies Publishing

Table 2. The performance comparison of different types of recent advanced solid electrolytes.

Types of solid electrolytes	Classification	Examples	Ionic Conductivity	Other Performance	Refs.
Sulfide-based SEs	Inorganic	Li_6PS_5Cl with EMG terpolymer	1.88 mS cm^{-1}	discharge capacity: 229.2 mA h g^{-1}	[126]
		$LiNi_xCo_yMn_{1-x-y}O_2$ (NCM) with Ni	/	discharge capacity: 193.2 mA h g^{-1} active mass loading: 26 mg cm^{-2}	[112]
		$LiF@Li_{10}GeP_2S_{12}$/ $F@Li_{10}GeP_2S_{12,}$	1.46×10^{-3} S cm^{-1}/ 2.21 mS cm^{-1}	initial discharge capacity:101.0 mAhg^{-1}/ critical current density:2.1 mA cm^{-2}	[127] [128]
Oxide-based SEs		$AlPO_4$-SiO_2-$Li_4P_2O_7$	1.63×10^{-6} to 1.68×10^{-4} mS cm^{-1}	High water stability	[129]
		OSE with PCE	0.25 mS cm^{-1}	Capacity retention: ~70% (After 820 h, at 0.1 °C)	[113]
Halide-based SEs		Li-VX_3 (X=Cl, Br, I)	/	Capacity retention: 85% (6 °C, > 200 cycles)	[114]
		(HNSEs) ZrO_2(−ACl)-A_2ZrCl_6 (A=Li or Na)	0.4 to 1.3 mS cm^{-1}	High-voltage stability and interfacial compatibility	[130]
Hydroborate/Boro-Based SEs		LLZ-$LiBH_4$	5.8×10^{-5} S cm^{-1}	Voltage endurance: 0.5 mA cm^{-2} (100 °C)	[131]
		$LiB_{11}H_{14}$	1.1×10^{-4} S cm^{-1} and 1.1×10^{-3} S cm^{-1}	Capacity retention: 82% (150 cycles. C/5)	[132]
Phosphide-based SEs		Li_3P, LiP, Li_3P_7, Li_3P_{11}, LiP_7, Li_4P_3, Li_5P_4, LiP_5	10^{-4} to 10^{-2} S cm^{-1}	Satisfactory stability, High lithium diffusion	[134]
		lithium-rich ternary phosphide	/	Low energy barrier and high efficiency of Li conduction	[133]
Solid Polymer Electrolytes (SPEs)	Organic	Combination of Li and LPIFD	3.0×10^{-4} S cm^{-1}	Critical current density: 3.7 mA cm^{-2}, Coulombic efficiency:99.1%	[135]
		PFVS	6.3×10^{-4} S cm^{-1}	Ionic mobility number: 0.82	[136]
Composite Polymer Electrolytes (CPEs)		PEO with LLZTO Composited	1.9×10^{-4} S cm^{-1}	Current density: 0.1 mA cm^{-2} (2000 h) Li$^+$ transference number: 0.67	[137]
		LiOTf, LLZTO, and PVDF/ PVAC Composited	5.09×10^{-4} S cm^{-1}	Capacity retention: 96% (180 cycles, 0.2 °C)	[138]
		Li with Nb-DRS	/	Capacity: 3 mAh cm^{-2}	[139]

The sol-gel method involves a series of processes, including gelling, drying, pressing, casting, and coating.[144] The prosecutor solves into the solvent and forms a prosecutor solution. The solution will then undergo a hydrolysis polymerization to form the sol solution. Depending on the purpose, the sol solution would perform different processes and result in various structures.[145] For instance, the wet gel can be obtained through grilling processing and then extracted from the aerogel after drying. In addition, through the precipitating, uniform particles can be obtained from the sol solution. Moreover, after spinning and the handling in furnace, ceramic fibers would be produced from sol solution.

5.1.2. Melt-Quenching

Melt-quenching is one of the traditional methods that is applied to produce glass materials, including bioactive glass, and glassy electrolytes (Figure 8a).[146] Melt-quenching involves several processes, including the handling of raw materials, the batch and melting process, the annealing process, and the shaping process. Before the process begins, the raw materials should be handled appropriately, and this process involves cleaning, selection, weighting, and mixing. After the preliminary process, the mixed materials would undergo the batch process. In this process, the materials heat up to a certain temperature and melt in a suitable container while stirring. The melt materials would be transported to the specific mold for casting and annealing. Before the shaping process, the annealed glass product would go through some preparation, including cutting, grinding, and polishing. Lastly, the glass would be characterized to the desired size and shape by different techniques.[148]

5.1.3. Mechanical Milling

Mechanical milling is a common top-down synthesis method that can be conducted with or without a solid-state chemical reaction.[149] Through the mechanical method, the dispersed powders are milled together, resulting in the formation of mechanochemical bonds.[150] Among the mechanical milling approaches, high-energy ball milling is commonly and widely
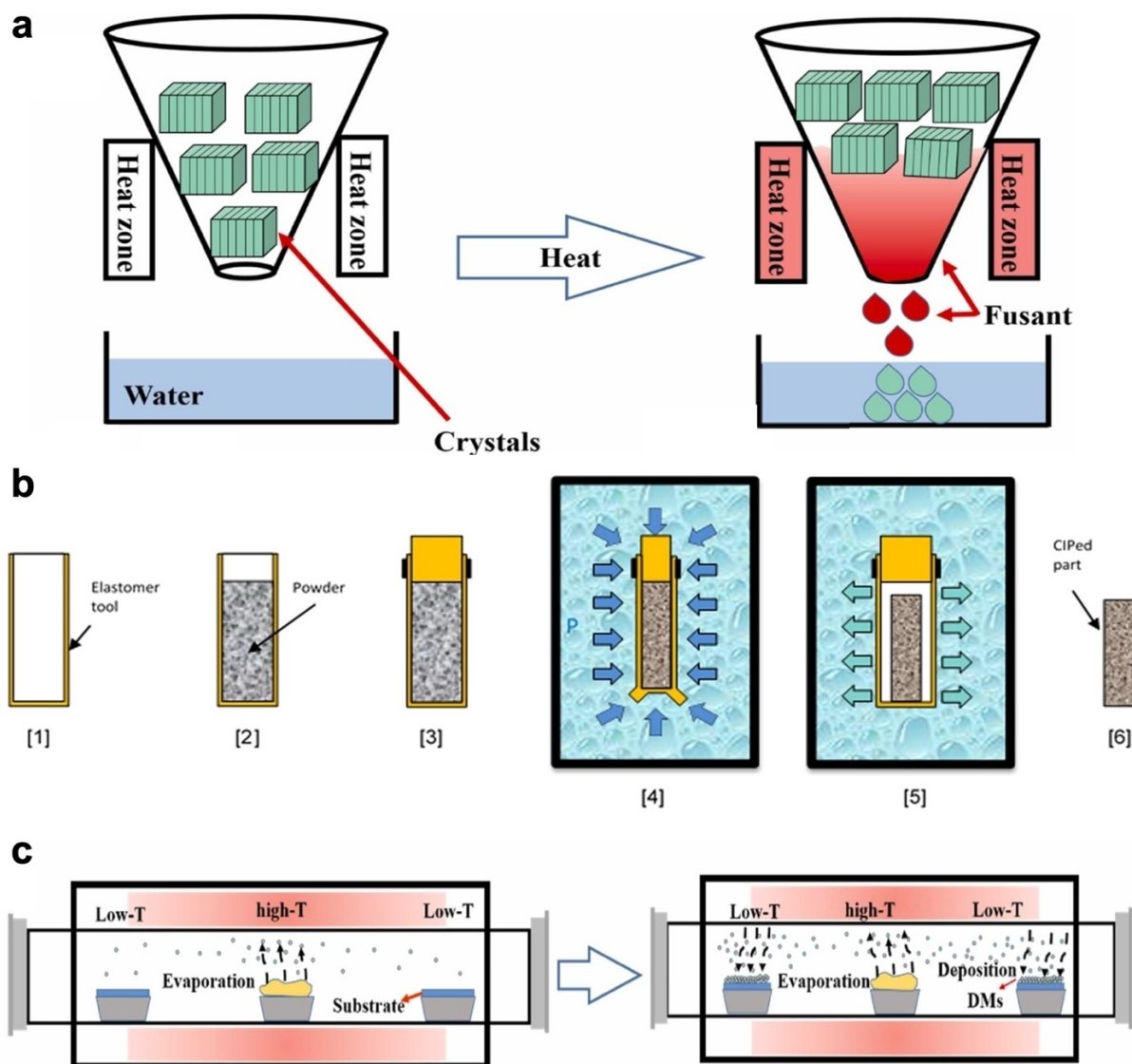
Batteries & Supercaps

Review
doi.org/10.1002/batt.202400432

Chemistry Europe
European Chemical
Societies Publishing

Figure 8. (a) The synthesis process of melt quenching. Reproduced with permission.[146] Copyright 2024 Elsevier. (b) The schematic diagram of the CIP process. Reproduced with permission.[147] Copyright 2021 Taylor & Francis. (c) The process of chemical vapor deposition (CVD). Reproduced with permission.[146] Copyright 2024 Elsevier.

applied for the synthesis. Mechanical milling can be employed to synthesize various types of materials for different applications, such as electrolytes, nanomaterials, and alloys. Mechanical milling involves a series of operations, including plastic deformation, cold welding, and fracture. These operations directly influence the characteristics of products: Plastic deformation controls the shape of particles, cold-welding increases the particle size and fracture reduces the particle size.

In the late 1960s, John Benjamin and his partner worked at the International Nickel Company, where they first developed the high-energy ball milling method to synthesize materials.[151] In this work, they successfully yielded the small, uniformly dispersed oxide particles (Al_2O_3, Y_2O_3, ThO_2) in nickel-base superalloys, where the traditional powder metallurgy methods are not able to provide the same performance. Afterward, they continuously studied and explored the application of mechan-

ical milling. In 1977, they reported that mechanical milling could produce metal composite, compounds, and other materials, except dispersion-strengthened alloys.[152]

5.2. Solid Polymer/Composite Electrolyte Synthesis

The presence of solid polymer electrolyte (SPE) broadens the electrochemical application of materials, such as fuel cells, supercapacitors, and high-energy-density rechargeable batteries.[153] In 1973, the first ion-conducting polymeric material was invented.[154] Afterward, the main goal of the researcher focuses on the synthesis of polymer electrolytes with room temperature ionic conductivity close to the liquid or aqueous electrolyte. Compared to the organic salt liquid, SPE has a lower room temperature ionic conductivity, but the usage of SPE is

Batteries & Supercaps

Review
doi.org/10.1002/batt.202400432

Chemistry Europe
European Chemical
Societies Publishing

safer. In addition, the shape versatility, flexibility, low-weight, and low processing costs, promising SPE to be useful materials for the lithium battery.

Although SPE possesses various advantages, some limitations still need to be overcome. One of the possible strategies is to combine SPE with other materials to synthesize composite electrolytes. Solid composite electrolyte (SCE) consists of the ionic conductor and the dielectric matrix. The engineering of the conduction interface can help to effectively increase the ionic conductivity.[155] The combinations of ionic conductors and matrix alter the molecular structure and increase the charge carrier concentration. These changes improve the ionic conductivity of the interface between the ionic conductor and matrix. The selection of synthesis would influence the properties of SPE/SCE.

5.2.1. Hot/Cold Isostatic Pressing

Isostatic pressing is a powder-based process for producing a solid electrolyte. Hot isostatic pressing (HIP) and cold isostatic pressing (CIP) are the traditional methods for the synthesis of solid-state electrolytes (Figure 8b).[147] The difference between HIP and CIP is the operation temperature. HIP conducts at elevated temperature, whereas CIP conducts at ambient temperature.[147,156] The isostatic pressing consists of different parts, including the elastomer tool, the powder-form material, the bung, and the pressure vessel. First, the powder-form material was placed into the elastomer tool. Afterward, the bung is used to close the tool. The following gentle vibration ensures the powder-form material to packedack until the material reaches the desired volume and density. The whole tool is placed into a pressure vessel to further compress by increasing the pressure of the vessel. In the end, the pressure is released gradually, and thereby, the shape of the tool retracts to its original form. The powder-from material converts to a partially dense compact.

5.2.2. Deposit Process

The deposit process is usually used to produce 2D materials, including thin film, transition metal chalcogenides, MXenes, electrolytes, and other materials. Chemical vapor deposition (CVD) and physical vapor deposition (PVD) are types of the deposit process (Figure 8c). These methods possess their specific advantages and limitations, where the main difference between the 2 methods is the coating process. PVD vapor vaporizes the liquid sources to gas through a physical reaction. The vapored gas then returns to solid form and coats the surface of the substrate. CVD uses a chemical reaction to produce the thin film, where the polymerization and the coating process conduct immediately.[157] The thin film produced by PVD is temperature resistant, where the film can withstand over 400 °C. The temperature resistance enables the applications for intense heat resistance.[158] In addition, PVD can produce very thin film with high abrasion and impact resistance. Moreover, PVD is an environmentally friendly technique, which implies it does not produce harmful by-products during the process. In contrast, CVD possesses specific advantages over PVD. First of all, CVD can synthesize the products with high purity, because most of the impurities would be eliminated by the airflow. Secondly, CVD uniformly coats the material to form an evenly distributed product. Finally, the overall cost of the CVD reaction is cheaper than the PVD.[159]

5.3. Direct Writing-Based 3D Printing

Direct writing-based 3D printing is a novel method for the synthesis of various materials, such as organic, inorganic, and composite materials. The 3D printing method is a type of additive manufacturing (AM), which is able to manufacture the materials with desired mechanical properties.[160] The appearance of the 3D printing method significantly accelerates the soft material design over the past decade.[161] Direct writing-based 3D printing method possesses some advantages, including high compatibility for the synthesis of a wide range of materials, and multiple crosslink methods. However, some limitations still need to be overcome, for instance, the challenges in the synthesis of materials with large overhanging structures, and relatively slow speed.[162] Nevertheless, 3D printing provides another available way to produce soft materials, such as electrolytes and polymers.

5.3.1. Direct Ink Writing

Direct ink writing (DIW) is extensively applied to manufacture architecture functional materials and biocompatible constructs.[163] Compared to other AM methods, DIW is the most general 3D printing method for the synthesis of various materials. As a type of extrusion-based AM method, DIW enables the production of meso- and microscale materials with complex structure and composition. The engineering of precursor ink leads to rheological behavior, therefore, DIW can produce practically any material.[168] In 1997, Cesarano and Calvert first applied DIW as a printing method to synthesize ceramic material with a complex structure at Sandia National Laboratory.[169] Afterward, more and more researchers studied and explored the application of DIW. The components of DIW commonly consist of the syringe, air pressure controller, air pump, and substrate (Figure 9a and b).[164] In the synthesis process, the raw material would convert to viscoelastic ink and then extrude through the deposition nozzle in a layer-by-layer form. The Computer-Aided-Design (CAD) software generates the 3D model of the product. Under computational control, the pathway of the deposition nozzle follows the design of a 3D model. During the movement process, the deposition nozzle discharges the ink and builds up the material with the desired scaffold.[170] The low cost, simplicity, and high versatility of DIW attract a massive number of scientists for the continuous state-of-the-art development of this technique.
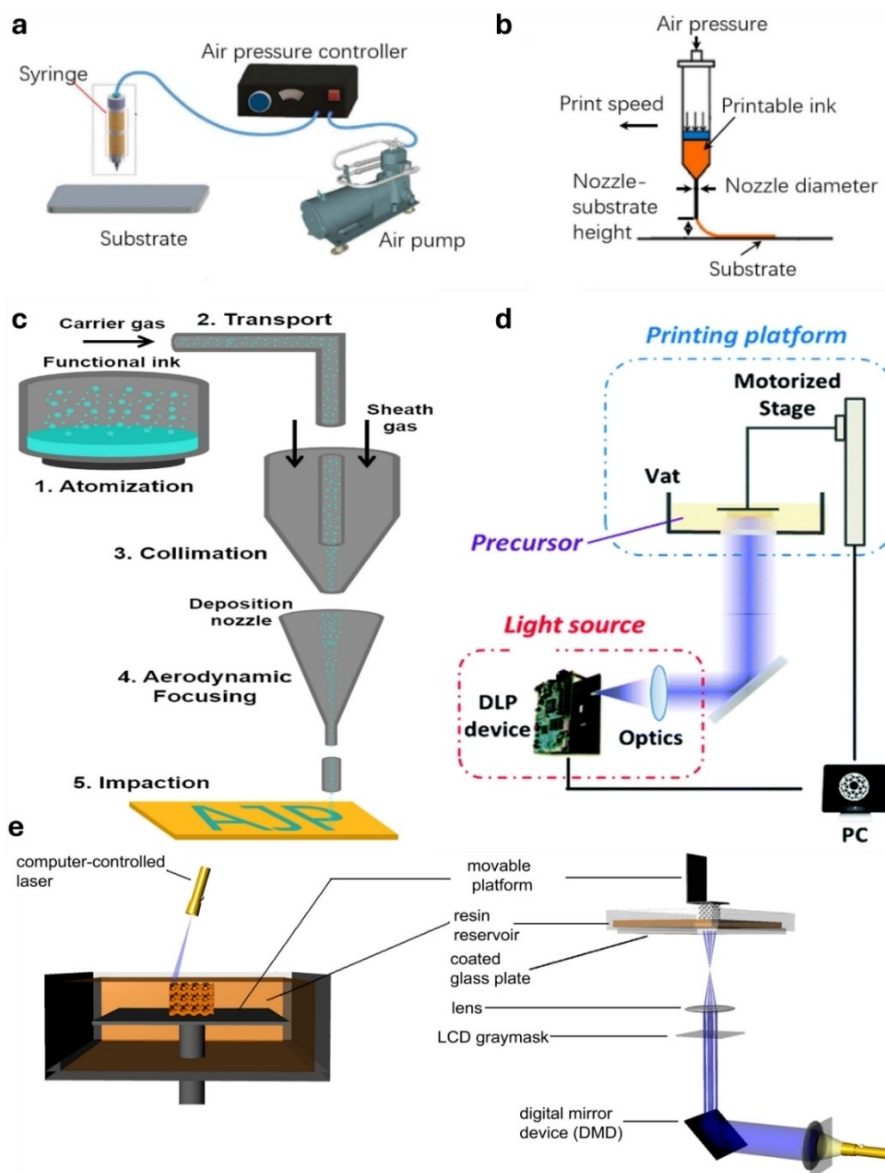
Batteries & Supercaps

Review
doi.org/10.1002/batt.202400432

Chemistry Europe
European Chemical
Societies Publishing

Figure 9. (a) The schematic diagram of the setup of DIW. (b) The basic process of the DIW. Reproduced with permission.[164] Copyright 2016 Nature. (c) The process of aerosol jet printing. Reproduced with permission.[165] Copyright 2018 IOP Science. (d) A representative setup of DLP-based printers. Reproduced with permission.[166] Copyright 2020 Royal Society of Chemistry. (e) The schemes of two types of stereolithography setups. Left: a bottom-up system with scanning laser. Right: a top-down setup with digital light projection. Reproduced with permission.[167] Copyright Elsevier B.V.

5.3.2. Aerosol Jet Printing

Aerosol jet printing (AJP) is a type of direct writing-based 3D printing method that deposits functional aerosolized solutions on free-form substrates.[171] Similar to other direct writing-based 3D printing methods, AJP can also promise fabrication techniques for different electrochemical devices. The AJP consists of several components, including the atomizer, the carrier gas, the mist transport channel, the deposition head, the nozzle, and the substrate.[172] The CAD software generates the motion data to control the AJP system. The atomizer converts the material to a dense mist droplet (ink). Afterward, the carrier gas (e.g. N_2 gas) transports the droplet through the transport

channel to the deposition head, where the nozzle deposits the droplet to the substrate to generate the product (Figure 9c).[165]

5.4. Lithography-Based 3D Printing

Besides direct writing-based 3D printing, lithography-based 3D printing is another printing method, which attracted interest from scientists over the past decade. Lithography-based 3D printing is intensively applied for material synthesis, including biomaterials, bio tissues, ceramics, and electrolytes.[173] Stereolithography and digital light processing are representative lithography-based 3D printing techniques. In this part, the

Batteries & Supercaps

Review
doi.org/10.1002/batt.202400432

Chemistry Europe
European Chemical
Societies Publishing

principle, and the relevant studies concerning the lithium solid-state electrolyte will be briefly discussed.

5.4.1. Digital Light Processing

Digital Light Processing (DLP) is a rapid 3D printing technique, which can build complex 3D materials through the deposition of raw materials. DLP can be used to produce soft materials, biomaterials, electronics, and other materials. The appearance of DLP provides a possible way to achieve high-resolution and elaborate 3D structures. The development of DLP can be traced back to 1977 when Dr. Larry Hornbeck studied the principles of reflection and manipulation of light.[174] In 1993, the prototype of DLP, Digital Imaging Division (DID) was developed. After the appearance of DLP, more and more efforts were further invented to develop the applications of DLP. The DLP printing component commonly consists of the printing platform (vat with precursor, motorized stage), the light source (DLP device, optics), and the computer. (Figure 9d)[166] The light source provides the energy and drives the light-sensitive reactants to start the reaction. The printing platform works as a dynamic container to contain the light-sensitive reactants and maintain the reaction environment. The DLP device (digital micromirror device with million pixels) and optics precisely reflect the incident projection light, control the light intensity, and provide satisfactory performance in terms of accuracy and printing speed.

5.4.2. Stereolithography

Stereolithography is a lithography-based 3D printing technique, where it utilizes photopolymerization to build the 3D structure in a layer-by-layer fashion. In other words, stereolithography solidifies the light-sensitive material of each layer.[175] The application of stereolithography is widespread, where it can be utilized for the building of biological products, ceramics, and other materials. Some limitations, such as the beam size and scan rate of the incident laser, would impact the sample resolution and the synthesis time.[176] To overcome the limitations of traditional stereolithography, new types of stereolithography were developed.

In the 1970s, the first significant work concerning stereolithography was conducted by Swainson, where both cross-linked and degraded polymers were synthesized by two intersecting radiation beams.[177] Afterward, the development of stereolithography can be classified into four generations. In 1984, the first generation, CW Hull employed laser scanning stereolithography to build 3D structure products.[177b] In the second generation, 1988, the projection stereolithography enable to cure of each layer immediately through the usage of photo mask technology. The usage of projection stereolithography overcomes the problem of low efficiency.[178] The third generation, Tumbleston et al.[179] applied continuous stereolithography to build the product in the scale of a minute. In 2016, the fourth generation, the appearance of volumetric stereolithography accelerated the building of 3D structures in the scale of seconds.

The setup of stereolithography can be classified into two types: (1) the bottom-up system with scanning laser, and (2) the top-down setup with digital light projection.[167] (Figure 9e) The bottom-up system applies the computer-controlled laser beam to decide the pattern and then constructs the product bottom-up on the support platform. The top-down system projects the light on the transparent, non-adhering plate from underneath. After the projection, the raw materials dip into the build platform from above and then construct the product.

6. Practical Challenges of ASSLBs

The study and application of ASSLBs demonstrate the potential to revolutionize the battery system and even the next-generation energy system in the future. The development of state-of-the-art ASSLBs benefits the battery system in terms of safety, energy density, lifetime, packaging, and the operable temperature range. Nevertheless, some practical challenges and obstacles to the further development of ASSLBS. For instance, the cost, scalability, interface property, and compatibility, are the main limitations that obstacle the development of ASSLBs.[180] These challenges should be addressed to transition the product from laboratory experiments to large-scale commercial applications. In this part, we will summarize the practical challenges of ASSLBs and the corresponding strategies in the following part.

6.1. Cost

The cost of developing an ASSLB is critical for expanding the application and transiting it from laboratory to commercial manufacturing. The synthesis method, raw material, time and electrical consumption, and personnel operation, are the critical factors that affect the overall cost of the final product. The expensive development cost may be an inescapable and unignorable hindrance for the large-scale commercial application of ASSLBs, even though the ASSLBs possess extraordinary properties. One of the examples is the battery for electric vehicles, where the cost of the LIBs dropped to USD 145 per kWh in around 2016.[181,182] The cost of the battery directly influences the final price of electric vehicles and then affects the desire of the customers to buy the electric vehicles. This challenge is an important issue for the laboratory which lacks the budget, especially in developing and backward countries.

In order to overcome the cost issue, researchers attempt to apply different methods for the lower development cost. One of the possible strategies is to substitute the original component with other cheaper materials to reduce the material cost. For instance, Roling and co-workers emphasized that using Sn to substitute Ge reduces the material cost by a factor of ~3 without an obvious reduction of total conductivity.[183] Another possible method is to simplify the manufactory process. For

Batteries & Supercaps

Review
doi.org/10.1002/batt.202400432

Chemistry
Europe
European Chemical
Societies Publishing

example, applying the electroplated Li metal could assist in the simplification of the manufacturing and lower the cost.[184] Moreover, the stability of SSE also influences the overall cost of the ASSLBs. The manufactory cost of air-sensitive SSEs is more expensive than the air-stable SSEs under ambient conditions. Controlling the ambient condition is an extra cost (~10%) during the manufactory process.[185]

6.2. Scalability

The growing demand for energy supply, storage, and relevant devices facilitates the development of large-scale ASSLBs. Along with the demand for large-scale energy supply, the safety requirement is not only focused on the small and isolated devices but also the large and multiple electrical devices and components. The safety regulatory requirements have become more demanding due to the increased scale of the electrical energy supply and storage.[186] As a result, the safety issue needs to be addressed to expand the scale of ASSLB production. In addition, the large-scale ASSLB manufactory is confronted with other problems. The high cost of the ASSLB product and the technological gaps lead to the difficulty of the transition from laboratory to large-scale manufacturing.[187]

The instability of some SSEs may cause the extra cost due to environmental control. For instance, the sulfide-based electrolyte is moisture-sensitive, and atmospheric moisture could cause chemical and mechanical degradation, therefore, leading to poor performance in terms of ionic conductivity and interfacial resistance.[188,189] Moreover, the reaction between the moisture and the sulfide (thiophosphates) may cause a hydrolysis reaction, and thereby, form the toxic H_2S.[182,190] The large-scale commercialization of these products requires a large budget to maintain a stable and safe condition, which hinders the large-scale manufactory. Furthermore, one of the typical synthesis methods of the sulfide SSEs is high-energy ball milling on the laboratory scale.[190,191] The technological gap limits the scale-up throughput and ease of processability from the laboratory scale to the manufactory on a large scale. The further development of relevant techniques would overcome the problems concerning scalability. Moreover, interfacial engineering may solve the problems concerning the cost and the technological gap.

6.3. Interface Property

The interface property is the heart of the solid-state battery, which involves physics, chemistry, and mechanics.[192] At the electrolyte-electrode interfaces, the interfacial electrochemical reactions drive the whole chemistry in the ASSLB.[193] As a result, the ionic conductivity of the ASSLB depends on the interfacial properties, including the wetting properties, the interface stability, the compatibility, and the migration speed of charge carriers across interfaces. The interface property of the ASSLBs could be influenced by these factors, including the rigid physical contact, the electrochemical/chemical interfacial reac-

tion, and the lithium dendrite growth and penetration.[190] To overcome these problems, interface engineering is applied to improve and develop the performance of the ASSLBs.

6.3.1. Rigid Physical Contact

The effective interaction area at the interface depends on the physical contact of the SE and the electrode. However, the rigid property of both SE and the electrode particles, and the rough surface of the particle, cause the point-to-point contact between them. The point-to-point contact causes poor contact and thus reduces the effective Li^+ migration areas between these materials.[194] Moreover, during the lithiation and delithiation processes, the rigid contact of these materials may cause uneven local stress and complex thermomechanical failures. The undesired stress and thermomechanic failures may finally cause the crack and delamination between the electrode and SE, and the direct broken of the SE layer.[195]

The electronic conduction of the cathode, Li anode, and the non-Li anode are different, where the Li anode possesses good electronic conductivity. Compared to the Li anode, the cathode and non-Li anode commonly consist of semiconductors or the composite, which possess relatively lower electronic conductivity than the Li anode.[196] Generally, the cathode material possesses the particle structure, which causes the void and the pore space, and therefore, causes poor contact at the interface. Besides the structure, the dynamic system of the ASSLBs may cause the chemomechanics induced failure on the surface of the electrolyte. During the operation, particle cracks, volume changes, and undesired chemical/mechanical reactions may occur on the surface due to the continuous change of the whole system. The volume change and particle crack induce the deformation of the electrolyte and thus produce strain on the surface of the electrolyte.[197] The appearance of strain alters the morphosis of the surface and affects the interfacial contact.

6.3.2. Electrochemical/Chemical Interfacial Reaction

Besides the rigid contact, the interfacial resistance caused by the sluggish charge transfer is another issue for the interface property.[190] At the interface, the irreversibly parasitic reactions would be caused by the excess electrode operating potentials over the electrochemical stability window. The excess electrode operating potentials cause the thermodynamic instability between the electrolyte and the electrode, and thus the parasitic reactions drive the formation of complex interphases, which possess high electronic conductivity or limited ionic conductivity and kinetic rate. Therefore, the parasitic reactions may obstacle the L+ transfer across the interfaces, and thus cause the poor performance of the cell.[198]

In the heterogeneous phase, the energetical favor of element exchange led to elemental interdiffusion, where the degree of interdiffusion is influenced by the mutual solubility and the diffusion coefficients. For the oxide-based SEs, this issue is common due to the co-sintering process under high

Batteries & Supercaps

Review
doi.org/10.1002/batt.202400432

Chemistry Europe
European Chemical
Societies Publishing

temperatures.[199] Besides the elemental interdiffusion, the redox, chemical, and electrochemical reactions at the interface are critical for interfacial stability. The dimension of the electrochemical stability window of the electrolyte depends on the gap between the highest occupied molecular orbital (HOMO) of the electrolytes and the lowest unoccupied molecular orbital (LUMO).[200] These reactions and the electrochemical stability directly affect the parasitic reaction and the formation of interphase.

6.3.3. Lithium Dendrite Growth and Penetration

In addition, at the SE/Li anode interface, the changing of Li dendrites and filaments leads to the short-circuit problem for the sulfide-based SE.[182] The potential safety risk caused by the short-circuit problem is considered as a challenge for the ASSLBs.[190] Generally, the uneven distribution of the Li and the contact loss are possible reasons for the safety issue. The enhancement of the Li protrusion could be achieved by the uneven electric field and Li^+ flux distribution, originating from the inhomogeneous interface.[201] Moreover, during the operation, the partial electronic conductivity of SEs may lead to the nucleation of Li inside the defect of sulfide-based SE.[202] Furthermore, the complexity and dynamic of the interface properties result from the changing of the solid interphase layer.[203]

The uniformity of Li on the surface depends on the plating and stripping. Also, the mechanical stress and strain affect the morphosis of the surface, and thereby, alter the uniformity and the formation of dendrites.[203] In some cases, high and low pressure is applied to the ASSLBs to increase the contact of solid components and prevent contact loss, preventively.[204] However, the application of pressure leads to the creep of Li, and hence, partial Li strip on the surface to cause the dendrite growth and short-circuit problem.[205] Moreover, the dendrite propagation and nucleation aggravate the short-circuit problem.[190] These processes increase the amount of Li dendrite in the whole battery. As the demand for ASSLBs increases, the safety issue is considered as the most important factor in the development of ASSLBs. Therefore, the safety issue concerning the short-circuit problem becomes complex and needs to be overcome for the various applications.

6.3.4. Interface Engineering

Interface engineering is an effective strategy to overcome the issues concerning the interface properties of ASSLBs. The interface engineering improves the interface stability and efficient charge carrier transport for high-energy and long-lifetime ASSLBs by managing the interface behavior. These methods require an in-depth understanding of the interface behavior and the mechanism of different problems.

6.3.4.1. Interface Engineering of the Cathode Side

The properties of the cathode active material are influenced by the composition, morphology, and microstructure of the cathode. In most cases, the microstructure of the cathode becomes unstable due to the volumetric variation. The stabilization of the microstructure reduces the volumetric variation during the operation. The low-strain and even zero-strain cathode is necessary to achieve the stability of the microstructure.[190] The blending method makes it possible to reduce the strain of the cathode by combining the materials with negative and positive stress. After the combination, the volume variation of the material can be partially and even completely canceled, and lead to a low/no net change of volume. Koerver et al.[190,197] combine NCM and $LiCoO_2$ materials to partially reduce the net change of the ASSLBs volume and thereby, the chemomechanical balance of the cell is improved due to the stability of the microstructure. In addition, the single crystalline structure is also useful to improve the microstructure of the cathode because of its satisfactory mechanical properties.[206]

The single crystalline cathode possesses enough mechanical stability, which ensures strength and improves the contact of the cathode. Moreover, the single crystalline cathode removes the intragranular boundaries, and thus, the barrier of the Li^+ and electron conductivity is directly eliminated, resulting in the enhancement of the charge carrier transfer.[207] Additionally, surface coating is another possible strategy to effectively improve the performance of the cathode in the ASSLBs. The coating directly changes the surface properties of the cathode, which may improve the compatibility, chemical stability, and ionic conductivity.[208]

6.3.4.2. Interface Engineering of the Anode Side

For the anode side, the interfacial buffer layer could be synthesized by the artificial interphase layer to adjust the interface properties. Commonly, the direct introduction of the additional buffer layer and the reaction between the Li and specific chemicals, are the general approaches to synthesize the protective layers on the surface of anode. The materials of the layer could be polymer (organic), inorganic, or a combination of them, which should be stable and compatible with the anode itself.[190] Besides the buffer layer, the solid electrolyte interphases (SEI) layer is another layer to improve the interface properties at the anode side. Theoretically, the SEI layer should be highly stable to avoid undesired parasitic reactions at the interface of the anode side. In order to prevent the formation of mixed conducting interphase (MIEC) interphase, the growth of dendrites, and the continuous change of the net volume, the SEI layer should contain high ionic conductivity, low electronic conductivity, satisfactory mechanical hardness, and enough elasticity.[209,210,209c]

In addition to the extra layer on the surface of the anode, doping could be applied to modify the property of the anode itself. The team of Han applied 30 % mol LiI to dope into the

Batteries & Supercaps | Review
doi.org/10.1002/batt.202400432

Chemistry
Europe
European Chemical
Societies Publishing

$Li_2S-P_2S_5$ glass and they finally improved the critical current density of the product to 3.9 mA cm^{-2} at 100 °C.[211] Similar to doping, the Li alloy is commonly used to enhance the performance of the anode. Compared to pure Li, the alloy Li could provide a lower diffusion barrier, and thus increase the diffusivity of Li$^+$. Benefitting from the increasing diffusivity, the deposition flux decreases and thus enhances the diffusion of Li on the surface of the electrode. As a result, the probability of the formation of dendrites on the surface of the anode would be reduced.[212]

7. Summary and Outlook

In conclusion, we summarize and review the background, the applications, and the developments of electrolytes in ASSLBs including sulfide-based electrolytes, oxide-based electrolytes, halide-based electrolytes, hydroborate-based electrolytes, phosphide-based electrolytes, solid polymer electrolytes, and the composite electrolytes. In addition, we have also reviewed recent studies and the performances of the representative electrolyte materials. More importantly, we have demonstrated the synthesis methods of different electrolytes, where the conventional chemical synthesis methods are systematically reviewed by the electrolyte types. Additionally, novel 3D printing methods including the direct writing-based and the lithography-based 3D printing methods are introduced for a better understanding of electrolyte synthesis. Besides, the relevant challenges of ASSLBs are summarized in this review.

Although different solid electrolytes have significantly improved the performance of lithium batteries, the research pace of electrolyte materials is still rapidly going forward. The demand for these electrolytes gradually increases with the development of new and renewable energy industries. The requirements, performance of the battery, and relevant devices, such as the efficiency, safety, environmentally friendly, and cost, are strived for progress by different researchers in the future. However, the challenges, such as scalability, cost, and interfacial resistance, limit the development of ASSLBs from the laboratory scale to the large-scale manufactory. For the interface property, the rigid physical contact, the electrochemical/chemical interfacial reaction, and the lithium dendrite growth and penetration are the main factors causing the challenge to develop the ASSLBs. Although these limitations obstacle the development and application of ASSLBS, the effort, and desire for the development and exploration of ASSLBs is still continuously increasing. Interface engineering, novel fabrication techniques, and new electrolyte/electrode materials are possible research directions to overcome these challenges.

Compared to the traditional lithium battery, the invention of ASSLBs provides a safer, improved energy density, higher ionic conductivity, longer lifetime, and higher capacity retention choice for the new energy supply and energy storage. The actual performance of the solid electrolyte is influenced by different factors, such as the composition, synthesis method, morphology, and size. Countless efforts are invested to discover the relationship between the factors and performance. As a result, the development and evolution of ASSLBs have shown obvious and explosive progress in recent years. The development of ASSLBs will be the milestone of another advanced technique in the future. The development of ASSLBs at this stage is meaningful, where the footprint of ASSLBs is the solid foundation of advanced techniques. The appearance of ASSLBs certainly improves sustainable developments and becomes the key to realizing environmentally friendly energy supply devices. It is expected that ASSLBs will be one of the main energy supplies in the future. This review will bring a clear and in-depth understanding of the solid electrolytes in lithium batteries, which further inspires the researchers to optimize the performances of ASSLBs towards practical applications with novel and advanced electrolytes.

Conflict of Interests

The authors declare no conflict of interest.

Keywords: Lithium battery · All-solid-state battery · Solid electrolyte · Classifications · Synthesis methods

[1] a) R. Schlögl, *Green Chem.* **2021**, *23*, 1584–1593; b) G. E. Blomgren, *J. Electrochem. Soc.* **2017**, *164*, A5019.
[2] Y. Nishi, *J. Power Sources* **2001**, *100*, 101–106.
[3] J.-L. Brédas, J. M. Buriak, F. Caruso, K.-S. Choi, B. A. Korgel, M. R. Palacín, K. Persson, E. Reichmanis, F. Schüth, R. Seshadri, M. D. Ward, *Chem. Mater.* **2019**, *31*, 8577–8581.
[4] S. Min, X. Liu, A. Wang, F. Ning, Y. Liu, J. Qin, J. Zhang, S. Lu, J. Yi, *Chin. Chem. Lett.* **2023**, *34*, 108586.
[5] A. Wang, J. Dai, Y. Guo, F. Ning, X. Liu, S. Subhan, J. Qin, S. Lu, J. Yi, *Chin. Chem. Lett.* **2024**, *34*, 110186.
[6] A. Wang, Y. Guo, F. Ning, X. Liu, F. Li, J. Zhang, S. Lu, J. Yi, *Energy Fuels* **2024**, *38*, 10324–10332.
[7] a) Y. Chen, Y. Kang, Y. Zhao, L. Wang, J. Liu, Y. Li, Z. Liang, X. He, X. Li, N. Tavajohi, B. Li, *J. Energy Chem.* **2021**, *59*, 83–99; b) C. T. Love, C. Buesser, M. D. Johannes, K. E. Swider-Lyons, *J. Electrochem. Energy Conver Storage* **2017**, *15*, 011006; c) D. P. Finegan, E. Darcy, M. Keyser, B. Tjaden, T. M. M. Heenan, R. Jervis, J. J. Bailey, N. T. Vo, O. V.

Magdysyuk, M. Drakopoulos, M. Di Michiel, A. Rack, G. Hinds, D. J. L. Brett, P. R. Shearing, *Adv. Sci.* **2018**, *5*, 1700369; d) B. Liu, J. Zhang, C. Zhang, J. Xu, *Eng. Failure Anal.* **2018**, *91*, 315–326; e) F. Schipper, E. M. Erickson, C. Erk, J.-Y. Shin, F. F. Chesneau, D. Aurbach, *J. Electrochem. Soc.* **2017**, *164*, A6220.

[8] S. Dong, L. Sheng, L. Wang, J. Liang, H. Zhang, Z. Chen, H. Xu, X. He, *Adv. Funct. Mater.* **2023**, *33*, 2304371.

[9] S. Chen, K. Wen, J. Fan, Y. Bando, D. Golberg, *J. Mater. Chem. A* **2018**, *6*, 11631–11663.

[10] B. L. Ellis, K. T. Lee, L. F. Nazar, *Chem. Mater.* **2010**, *22*, 691–714.

[11] a) N. Phattharasupakun, P. Bunyanidhi, P. Chiochan, N. Chanlek, M. Sawangphruk, *Electrochem. Commun.* **2022**, *139*, 107309; b) J. H. Choi, S. Choi, T. J. Embleton, K. Ko, K. S. Saqib, M. Jo, J. Hwang, S. Park, Y. Son, P. Oh, *Batteries* **2023**, *9*, 590

[12] L. Ma, Y. Dong, N. Li, W. Yan, S. Ma, Y. Fang, Y. Li, L. Xu, C. Liu, S. Chen, R. Feng, L. Chen, D. Cao, Y. Lu, Q. Huang, Y. Su, F. Wu, *eTransportation* **2024**, *20*, 100312.

[13] C. Cao, Z.-B. Li, X.-L. Wang, X.-B. Zhao, W.-Q. Han, *Front. Energy Res.* **2014**, *2*, 25.

[14] G. Xi, M. Xiao, S. Wang, D. Han, Y. Li, Y. Meng, *Adv. Funct. Mater.* **2021**, *31*, 2007598.

[15] M. Dirican, C. Yan, P. Zhu, X. Zhang, *Mater. Sci. Eng. R* **2019**, *136*, 27–46.

[16] J. Gao, S.-Q. Shi, H. Li, *Chin. Phys. B* **2016**, *25*, 018210.

[17] S. Chai, Q. He, J. Zhou, Z. Chang, A. Pan, H. Zhou, *ChemSusChem* **2024**, *17*, e202301268.

[18] L. Fan, S. Wei, S. Li, Q. Li, Y. Lu, *Adv. Energy Mater.* **2018**, *8*, 1702657.

[19] S. Xia, X. Wu, Z. Zhang, Y. Cui, W. Liu, *Chem* **2019**, *5*, 753–785.

[20] a) J. Liu, T. Wang, J. Yu, S. Li, H. Ma, X. Liu, *Materials* **2023**, *16*, 2510; b) V. Kumaravel, J. Bartlett, S. C. Pillai, *Adv. Energy Mater.* **2021**, *11*, 2002869

[21] Y. Wang, W. D. Richards, S. P. Ong, L. J. Miara, J. C. Kim, Y. Mo, G. Ceder, *Nat. Mater.* **2015**, *14*, 1026–1031.

[22] M. Petrowsky, R. Frech, *J. Phys. Chem. B* **2009**, *113*, 5996–6000.

[23] A. Manthiram, X. Yu, S. Wang, *Nat. Rev. Mater.* **2017**, *2*, 16103.

[24] J. B. Goodenough, H. Y. P. Hong, J. A. Kafalas, *Mater. Res. Bull.* **1976**, *11*, 203–220.

[25] K. Liu, R. Zhang, J. Sun, M. Wu, T. Zhao, *ACS Appl. Mater. Interfaces* **2019**, *11*, 46930–46937.

[26] a) M. Guin, F. Tietz, O. Guillon, *Solid State Ionics* **2016**, *293*, 18–26; b) Q. Ma, M. Guin, S. Naqash, C.-L. Tsai, F. Tietz, O. Guillon, *Chem. Mater.* **2016**, *28*, 4821–4828; c) M. Guin, E. Dashjav, C. M. N. Kumar, F. Tietz, O. Guillon, *Solid State Sci.* **2017**, *67*, 30–36

[27] Y. Li, M. Liu, K. Liu, C.-A. Wang, *J. Power Sources* **2013**, *240*, 50–53.

[28] a) J. C. Bachman, S. Muy, A. Grimaud, H.-H. Chang, N. Pour, S. F. Lux, O. Paschos, F. Maglia, S. Lupart, P. Lamp, L. Giordano, Y. Shao-Horn, *Chem. Rev.* **2016**, *116*, 140–162; b) B. Zhang, R. Tan, L. Yang, J. Zheng, K. Zhang, S. Mo, Z. Lin, F. Pan, *Energy Storage Mater.* **2018**, *10*, 139–159.

[29] A. G. Belous, *J. Eur. Ceram. Soc.* **2001**, *21*, 1797–1800.

[30] a) S. Yan, C.-H. Yim, V. Pankov, M. Bauer, E. Baranova, A. Weck, A. Merati, Y. Abu-Lebdeh, *Batteries*, **2021**, *7*, 75; b) J. Lu, Y. Li, *J. Mater. Sci. Mater. Electron.* **2021**, *32*, 9736–9754.

[31] K. Mitsuishi, T. Ohnishi, Y. Tanaka, K. Watanabe, I. Sakaguchi, N. Ishida, M. Takeguchi, T. Ohno, D. Fujita, K. Takada, *Appl. Phys. Lett.* **2012**, *101*, 073903.

[32] G.-Y. Adachi, N. Imanaka, S. Tamura, *Chem. Rev.* **2002**, *102*, 2405–2430.

[33] H.-T. Chung, J.-G. Kim, H.-G. Kim, *Solid State Ionics* **1998**, *107*, 153–160.

[34] L. Xu, T. Feng, J. Huang, Y. Hu, L. Zhang, L. Luo, *ACS Appl. Energ. Mater.* **2022**, *5*, 3741–3747.

[35] H. Xu, P.-H. Chien, J. Shi, Y. Li, N. Wu, Y. Liu, Y.-Y. Hu, J. B. Goodenough, *Proc. Natl. Acad. Sci. USA* **2019**, *116*, 18815–18821.

[36] a) J.-F. Wu, W. K. Pang, V. K. Peterson, L. Wei, X. Guo, *ACS Appl. Mater. Interfaces* **2017**, *9*, 12461–12468; b) R. Murugan, V. Thangadurai, W. Weppner, *Angew. Chem. Int. Ed.* **2007**, *46*, 7778–7781; c) V. Thangadurai, S. Narayanan, D. Pinzaru, *Chem. Soc. Rev.* **2014**, *43*, 4714–4727.

[37] A. Kim, S. Woo, M. Kang, H. Park, B. Kang, *Front. Chem.* **2020**, *8*, 468.

[38] K. Hofstetter, A. J. Samson, J. Dai, J. E. Gritton, L. Hu, E. D. Wachsman, V. Thangadurai, *J. Electrochem. Soc.* **2019**, *166*, A1844.

[39] a) L. Yang, X. Tao, X. Huang, C. Zou, L. Yi, X. Chen, Z. Zang, Z. Luo, X. Wang, *ACS Appl. Mater. Interfaces* **2021**, *13*, 56054–56063; b) N. C. Rosero-Navarro, T. Yamashita, A. Miura, M. Higuchi, K. Tadanaga, *J. Am. Ceram. Soc.* **2017**, *100*, 276–285.

[40] J. Awaka, N. Kijima, H. Hayakawa, J. Akimoto, *J. Solid State Chem.* **2009**, *182*, 2046–2052.

[41] M. Kim, H. G. Park, K. Park, *Phys. Chem. Chem. Phys.* **2022**, *24*, 29159–29164.

[42] L. J. Miara, W. D. Richards, Y. E. Wang, G. Ceder, *Chem. Mater.* **2015**, *27*, 4040–4047.

[43] S. Ohta, J. Seki, Y. Yagi, Y. Kihira, T. Tani, T. Asaoka, *J. Power Sources* **2014**, *265*, 40–44.

[44] W. Shu, Z. Jian, J. Zhou, Y. Zheng, W. Chen, *ACS Appl. Mater. Interfaces* **2021**, *13*, 54916–54923.

[45] C. Shen, Y. Liu, W. Li, X. Liu, J. Xie, J. Jiang, Y. Jiang, B. Zhao, J. Zhang, *J. Colloid Interface Sci.* **2022**, *615*, 1–9.

[46] W. Luo, Y. Gong, Y. Zhu, K. K. Fu, J. Dai, S. D. Lacey, C. Wang, B. Liu, X. Han, Y. Mo, E. D. Wachsman, L. Hu, *J. Am. Chem. Soc.* **2016**, *138*, 12258–12262.

[47] L. Cheng, C. H. Wu, A. Jarry, W. Chen, Y. Ye, J. Zhu, R. Kostecki, K. Persson, J. Guo, M. Salmeron, G. Chen, M. Doeff, *ACS Appl. Mater. Interfaces* **2015**, *7*, 17649–17655.

[48] a) S. Qin, X. Zhu, Y. Jiang, M. e. Ling, Z. Hu, J. Zhu, *Appl. Phys. Lett.* **2018**, *112*, 113901; b) H. Aono, E. Sugimoto, Y. Sadaoka, N. Imanaka, G. y. Adachi, *J. Electrochem. Soc.* **1990**, *137*, 1023.

[49] J. Shao, Z. Li, Y. Zeng, S. Chen, L. Yang, H. Zhang, *J. Alloys Compd.* **2020**, *816*, 152517.

[50] a) Z. Q. Wang, M. S. Wu, G. Liu, X. L. Lei, B. Xu, C. Y. Ouyang, *Int. J. Electrochem. Sci.* **2014**, *9*, 562–568; b) M. Papakyriakou, M. Lu, Y. Liu, Z. Liu, H. Chen, M. T. McDowell, S. Xia, *J. Power Sources* **2021**, *516*, 230672.

[51] M. Tatsumisago, M. Nagao, A. Hayashi, *J. Asian Ceram. Soc.* **2013**, *1*, 17–25.

[52] a) R. Mercier, J.-P. Malugani, B. Fahys, G. Robert, *Solid State Ionics* **1981**, *5*, 663–666; b) H. Wada, M. Menetrier, A. Levasseur, P. Hagenmuller, *Mater. Res. Bull.* **1983**, *18*, 189–193; c) V. K. Deshpande, A. Pradel, M. Ribes, *Mater. Res. Bull.* **1988**, *23*, 379–384; d) M. Tachez, J.-P. Malugani, R. Mercier, G. Robert, *Solid State Ionics* **1984**, *14*, 181–185.

[53] Y. Seino, T. Ota, K. Takada, A. Hayashi, M. Tatsumisago, *Energy Environ. Sci.* **2014**, *7*, 627–631.

[54] W. D. Jung, J.-S. Kim, S. Choi, S. Kim, M. Jeon, H.-G. Jung, K. Y. Chung, J.-H. Lee, B.-K. Kim, J.-H. Lee, H. Kim, *Nano Lett.* **2020**, *20*, 2303–2309.

[55] Y. Lee, J. Jeong, H. J. Lee, M. Kim, D. Han, H. Kim, J. M. Yuk, K.-W. Nam, K. Y. Chung, H.-G. Jung, S. Yu, *ACS Energy Lett.* **2022**, *7*, 171–179.

[56] N. Kamaya, K. Homma, Y. Yamakawa, M. Hirayama, R. Kanno, M. Yonemura, T. Kamiyama, Y. Kato, S. Hama, K. Kawamoto, A. Mitsui, *Nat. Mater.* **2011**, *10*, 682–686.

[57] S. Jian, H. Li, X. Jia, D. Zhong, B. Tao, X. He, G. Wang, H. Chang, *FlatChem* **2024**, *46*, 100693.

[58] K.-H. Park, K. Kaup, A. Assoud, Q. Zhang, X. Wu, L. F. Nazar, *ACS Energy Lett.* **2020**, *5*, 533–539.

[59] S. Y. Kim, K. Kaup, K.-H. Park, A. Assoud, L. Zhou, J. Liu, X. Wu, L. F. Nazar, *ACS Materials Lett.* **2021**, *3*, 930–938.

[60] Y. Li, S. Song, H. Kim, K. Nomoto, H. Kim, X. Sun, S. Hori, K. Suzuki, N. Matsui, M. Hirayama, T. Mizoguchi, T. Saito, T. Kamiyama, R. Kanno, *Science* **2023**, *381*, 50–53.

[61] S. Wang, S. Liu, W. Chen, Y. Hu, D. Chen, M. He, M. Zhou, T. Lei, Y. Zhang, J. Xiong, *Adv. Sci.* **2024**, *11*, 2401889.

[62] Y. Kato, S. Hori, T. Saito, K. Suzuki, M. Hirayama, A. Mitsui, M. Yonemura, H. Iba, R. Kanno, *Nat. Energy* **2016**, *1*, 16030.

[63] K. Hikima, K. Ogawa, H. Gamo, A. Matsuda, *Chem. Commun.* **2023**, *59*, 6564–6567.

[64] C. Fan, N. Ahmad, T. Song, C. Zeng, X. Liang, Q. Dong, W. Yang, *Nano Res.* **2024**, DOI: 10.1007/s12274-024-6871-3.

[65] a) T. Asano, A. Sakai, S. Ouchi, M. Sakaida, A. Miyazaki, S. Hasegawa, *Adv. Mater.* **2018**, *30*, 1803075; b) Y. Subramanian, R. Rajagopal, K.-S. Ryu, *ACS Appl. Mater. Interfaces* **2024**, *16*, 24534–24546.

[66] a) C. Li, L. Gu, J. Maier, *Adv. Funct. Mater.* **2012**, *22*, 1145–1149; b) C. Li, L. Gu, X. Guo, D. Samuelis, K. Tang, J. Maier, *Nano Lett.* **2012**, *12*, 1241–1246.

[67] Y. Zhu, Y. Mo, *Angew. Chem. Int. Ed.* **2020**, *59*, 17472–17476.

[68] a) D. Park, H. Park, Y. Lee, S.-O. Kim, H.-G. Jung, K. Y. Chung, J. H. Shim, S. Yu, *ACS Appl. Mater. Interfaces* **2020**, *12*, 34806–34814; b) S. Wang, Q. Bai, A. M. Nolan, Y. Liu, S. Gong, Q. Sun, Y. Mo, *Angew. Chem. Int. Ed.* **2019**, *58*, 8039–8043.

[69] a) M. Feinauer, H. Euchner, M. Fichtner, M. A. Reddy, *ACS Appl. Energ. Mater.* **2019**, *2*, 7196–7203; b) E. Umeshbabu, S. Maddukuri, Y. Hu, M. Fichtner, A. R. Munnangi, *ACS Appl. Mater. Interfaces* **2022**, *14*, 25448–25456.

[70] T. Oi, K. Miyauchi, *Mater. Res. Bull.* **1981**, *16*, 1281–1289.

[71] a) C. Zhao, J. Liang, X. Li, N. Holmes, C. Wang, J. Wang, F. Zhao, S. Li, Q. Sun, X. Yang, J. Liang, X. Lin, W. Li, R. Li, S. Zhao, H. Huang, L. Zhang, S. Lu, X. Sun, *Nano Energy* **2020**, *75*, 105036; b) X. Shi, Z. Zeng, M. Sun, B.

Huang, H. Zhang, W. Luo, Y. Huang, Y. Du, C. Yan, *Nano Lett.* **2021**, *21*, 9325–9331.

[72] J. Liang, X. Li, K. R. Adair, X. Sun, *Acc. Chem. Res.* **2021**, *54*, 1023–1033.

[73] a) S. Muy, J. Voss, R. Schlem, R. Koerver, S. J. Sedlmaier, F. Maglia, P. Lamp, W. G. Zeier, Y. Shao-Horn, *iScience* **2019**, *16*, 270–282; b) Z. Xu, X. Chen, K. Liu, R. Chen, X. Zeng, H. Zhu, *Chem. Mater.* **2019**, *31*, 7425–7433; c) Y. Liu, S. Wang, A. M. Nolan, C. Ling, Y. Mo, *Adv. Energy Mater.* **2020**, *10*, 2002356; d) M. Gombotz, H. M. R. Wilkening, *ACS Sustainable Chem. Eng.* **2021**, *9*, 743–755.

[74] J. Park, D. Han, H. Kwak, Y. Han, Y. J. Choi, K.-W. Nam, Y. S. Jung, *Chem. Eng. J.* **2021**, *425*, 130630.

[75] a) C. Wang, J. Liang, J. Luo, J. Liu, X. Li, F. Zhao, R. Li, H. Huang, S. Zhao, L. Zhang, J. Wang, X. Sun, *Sci. Adv.* **2021**, *7*, eabh1896; b) E. Sebti, H. A. Evans, H. Chen, P. M. Richardson, K. M. White, R. Giovine, K. P. Koirala, Y. Xu, E. Gonzalez-Correa, C. Wang, C. M. Brown, A. K. Cheetham, P. Canepa, R. J. Clément, *J. Am. Chem. Soc.* **2022**, *144*, 5795–5811

[76] S. Wang, X. Xu, C. Cui, C. Zeng, J. Liang, J. Fu, R. Zhang, T. Zhai, H. Li, *Adv. Funct. Mater.* **2022**, *32*, 2108805.

[77] X. Li, J. Liang, J. Luo, M. Norouzi Banis, C. Wang, W. Li, S. Deng, C. Yu, F. Zhao, Y. Hu, T.-K. Sham, L. Zhang, S. Zhao, S. Lu, H. Huang, R. Li, K. R. Adair, X. Sun, *Energy Environ. Sci.* **2019**, *12*, 2665–2671.

[78] R. N. Grimes, *Carboranes*, Academic Press **2016**.

[79] L. Schlapbach, A. Züttel, *Nature* **2001**, *414*, 353–358.

[80] a) J. Cuan, Y. Zhou, T. Zhou, S. Ling, K. Rui, Z. Guo, H. Liu, X. Yu, *Adv. Mater.* **2019**, *31*, 1803533; b) Z. Lu, F. Ciucci, *Chem. Mater.* **2017**, *29*, 9308–9319.

[81] a) P. Till, R. Asakura, A. Remhof, W. G. Zeier, *J. Phys. Chem. C* **2023**, *127*, 987–993; b) M. Brighi, F. Murgia, R. Černý, *Adv. Mater. Interfaces* **2022**, *9*, 2101254; c) M. Jin, S. Cheng, Z. Yang, Y. Luo, Y. Guo, *Chem. Eng. J.* **2023**, *455*, 140904; d) C. Zhou, Y. Yan, T. R. Jensen, *ACS Appl. Energy Mater.* **2023**, *6*, 7346–7352

[82] A. Dey, J. Miller, *J. Electrochem. Soc.* **1979**, *126*, 1445.

[83] M. Matsuo, Y. Nakamori, S.-I Orimo, H. Maekawa, H. Takamura, *Appl. Phys. Lett.* **2007**, *91*, 224103.

[84] a) M. Matsuo, H. Takamura, H. Maekawa, H.-W. Li, S.-i. Orimo, *Appl. Phys. Lett.* **2009**, *94*; b) T. Ikeshoji, E. Tsuchida, T. Morishita, K. Ikeda, M. Matsuo, Y. Kawazoe, S.-i. Orimo, *Phys. Rev. B* **2011**, *83*, 144301; c) P. Martelli, A. Remhof, A. Borgschulte, R. Ackermann, T. Strassle, J. P. Embs, M. Ernst, M. Matsuo, S.-I. Orimo, A. Züttel, *J. Phys. Chem. A* **2011**, *115*, 5329–5334

[85] W. S. Tang, K. Yoshida, A. V. Soloninin, R. V. Skoryunov, O. A. Babanova, A. V. Skripov, M. Dimitrievska, V. Stavila, . Orimo, T. J. Udovic, *ACS Energy Lett.* **2016**, *1*, 659–664.

[86] M. Jin, D. Xu, Z. Su, Z. He, X. Chen, R. Wu, Y. Guo, *ACS Energy Lett.* **2024**, *9*, 1176–1183.

[87] S. Payandeh, D. Rentsch, Z. Łodziana, R. Asakura, L. Bigler, R. Černý, C. Battaglia, A. Remhof, *Adv. Funct. Mater.* **2021**, *31*, 2010046.

[88] N. N. Greenwood, A. Earnshaw, *Chemistry of the Elements*, Elsevier **2012**.

[89] R. Pöttgen, W. Hönle, H. G. von Schnering, *Encycl. Inorg. Chem.* 2006, R. B. King, New York, John Wiley & Sons, Ltd. .

[90] G. S. Bumbrah, K. Krishan, T. Kanchan, M. Sharma, G. S. Sodhi, *Forensic Sci. Int.* **2012**, *214*, 1–6.

[91] Y. Fu, O. Wei, G. Zhang, S. Sun, *Adv. Energy Mater.* **2018**, *8*, 1703058.

[92] J. Shim, L. Kim, H. J. Kim, D. Jeong, J. H. Lee, J.-C. Lee, *Polymer* **2017**, *122*, 222–231.

[93] Y. Chen, Y. Shi, Y. Liang, H. Dong, F. Hao, A. Wang, Y. Zhu, X. Cui, Y. Yao, *ACS Appl. Energ. Mater.* **2019**, *2*, 1608–1615.

[94] J. Zhou, Q. Shi, S. Ullah, X. Yang, A. Bachmatiuk, R. Yang, M. H. Rummeli, *Adv. Funct. Mater.* **2020**, *30*, 2004648.

[95] S. Liu, H. Zhang, L. Xu, L. Ma, X. Chen, *J. Power Sources* **2016**, *304*, 346–353.

[96] a) R. Khurana, J. L. Schaefer, L. A. Archer, G. W. Coates, *J. Am. Chem. Soc.* **2014**, *136*, 7395–7402; b) Z. Zhao, Y. Zhang, S. Li, S. Wang, Y. Li, H. Mi, L. Sun, X. Ren, P. Zhang, *J. Mater. Chem. A* **2019**, *7*, 25818–25823.

[97] S. Huo, L. Sheng, W. Xue, L. Wang, H. Xu, H. Zhang, X. He, *InfoMat* **2023**, *5*, e12394.

[98] Z. Shen, Y. Cheng, S. Sun, X. Ke, L. Liu, Z. Shi, *Carbon Energy* **2021**, *3*, 482–508.

[99] W. H. Meyer, *Adv. Mater.* **1998**, *10*, 439–448.

[100] Y. Wang, W.-H. Zhong, *ChemElectroChem* **2015**, *2*, 22–36.

[101] X.-G. Sun, J. B. Kerr, *Macromolecules* **2006**, *39*, 362–372.

[102] H. Zhang, C. Li, M. Piszcz, E. Coya, T. Rojo, L. M. Rodriguez-Martinez, M. Armand, Z. Zhou, *Chem. Soc. Rev.* **2017**, *46*, 797–815.

[103] Y. Li, K. W. Wong, Q. Dou, K. M. Ng, *J. Mater. Chem. A* **2016**, *4*, 18543–18550.

[104] Y. Jiang, X. Yan, Z. Ma, P. Mei, W. Xiao, Q. You, Y. Zhang, *Polymers* **2018**, *10*, 1237.

[105] a) T. Ogoshi, R. Sueto, M. Yagyu, R. Kojima, T. Kakuta, T.-a. Yamagishi, K. Doitomi, A. K. Tummanapelli, H. Hirao, Y. Sakata, S. Akine, M. Mizuno, *Nat. Commun.* **2019**, *10*, 479; b) V. St-Onge, S. Rochon, J.-C. Daigle, A. Soldera, J. P. Claverie, *Angew. Chem. Int. Ed.* **2021**, *60*, 25897–25904.

[106] a) E. Tsuchida, H. Ohno, K. Tsunemi, N. Kobayashi, *Solid State Ionics* **1983**, *11*, 227–233; b) S. Holappa, L. Kantonen, F. M. Winnik, H. Tenhu, *Macromolecules* **2004**, *37*, 7008–7018.

[107] a) A. Paajanen, J. Vaari, T. Verho, *Polymer* **2019**, *171*, 80–86; b) N. Wang, Y. Wei, S. Yu, W. Zhang, X. Huang, B. Fan, H. Yuan, Y. Tan, *J. Mater. Sci. Technol.* **2024**, *183*, 206–214.

[108] P. Fan, H. Liu, V. Marosz, N. T. Samuels, S. L. Suib, L. Sun, L. Liao, *Adv. Funct. Mater.* **2021**, *31*, 2101380.

[109] a) X. Yang, J. Liu, N. Pei, Z. Chen, R. Li, L. Fu, P. Zhang, J. Zhao, *Nano-Micro Lett.* **2023**, *15*, 74; b) Q. Yu, K. Jiang, C. Yu, X. Chen, C. Zhang, Y. Yao, B. Jiang, H. Long, *Chin. Chem. Lett.* **2021**, *32*, 2659–2678.

[110] R. Chen, W. Qu, X. Guo, Li, F. Wu, *Mater. Horiz.* **2016**, *3*, 487–516.

[111] a) K. He, S. H.-S. Cheng, J. Hu, Y. Zhang, H. Yang, Y. Liu, W. Liao, D. Chen, C. Liao, X. Cheng, Z. Lu, J. He, J. Tang, R. K. Y. Li, C. Liu, *Angew. Chem. Int. Ed.* **2021**, *60*, 12116–12123; b) J. Cheng, G. Hou, Q. Chen, D. Li, K. Li, Q. Yuan, J. Wang, L. Ci, *Chem. Eng. J.* **2022**, *429*, 132343; c) J. A. Isaac, D. Devaux, R. Bouchet, *Nat. Mater.* **2022**, *21*, 1412–1418.

[112] S. B. Hong, Y. J. Lee, H. J. Lee, H. T. Sim, H. Lee, Y. M. Lee, D. W. Kim, *Small* **2024**, *20*, 2304747.

[113] H. Sun, Z. Liu, M. Xin, Y. Shi, Y. Wang, S. Ma, X. Yang, H. Xie, Y. Liu, *J. Colloid Interface Sci.* **2024**, *653*, 908–916.

[114] J. Liang, X. Li, J. T. Kim, X. Hao, H. Duan, R. Li, X. Sun, *Angew. Chem.* **2023**, *135*, e202217081.

[115] J. Li, Shen, *ACS Appl. Polym. Mater.* **2022**, *4*, 7144–7151.

[116] J.-K. Kim, L. Aguilera, F. Croce, J.-H. Ahn, *J. Mater. Chem. A* **2014**, *2*, 3551–3556.

[117] S. Hua, J.-l. Li, M.-x. Jing, F. Chen, B.-w. Ju, F.-y. Tu, X.-q. Shen, S.-b. Qin, *Int. J. Energy Res.* **2020**, *44*, 6452–6462.

[118] C. Wang, T. Yang, W. Zhang, H. Huang, Y. Gan, Y. Xia, X. He, J. Zhang, *J. Mater. Chem. A* **2022**, *10*, 3400–3408.

[119] L. Chen, Y. Li, S.-P. Li, L.-Z. Fan, C.-W. Nan, J. B. Goodenough, *Nano Energy* **2018**, *46*, 176–184.

[120] Z. Gao, H. Sun, L. Fu, F. Ye, Y. Zhang, W. Luo, Y. Huang, *Adv. Mater.* **2018**, *30*, 1705702.

[121] a) Y. Zhao, Z. Huang, S. Chen, B. Chen, J. Yang, Q. Zhang, F. Ding, Y. Chen, X. Xu, *Solid State Ionics* **2016**, *295*, 65–71; b) W. Wang, E. Yi, A. J. Fici, R. M. Laine, J. Kieffer, *J. Phys. Chem. C* **2017**, *121*, 2563–2573.

[122] a) Z. Tian, D. Kim, *J. Energy Chem.* **2022**, *68*, 603–611; b) G. Tian, H. Li, B. Khalid, Z. Zhao, *Chem. Eng. J.* **2022**, *430*, 132803.

[123] R. Li, Z. Fang, C. Wang, X. Zhu, X. Fu, J. Fu, W. Yan, Y. Yang, *Chem. Eng. J.* **2022**, *430*, 132706.

[124] M. Latifi, A. Ahmad, N. H. Hassan, *Mater. Today: Proc.* **2021**, *36*, 16–21.

[125] Y. Zhao, R. Tao, T. Fujinami, *Electrochim. Acta* **2006**, *51*, 6451–6455.

[126] S.-B. Hong, Y.-R. Jang, Y.-C. Jung, W. Cho, D.-W. Kim, *ACS Appl. Energy Mater.* **2024**, *7*, 5193–5201.

[127] Y. Jin, Q. He, G. Liu, Z. Gu, M. Wu, T. Sun, Z. Zhang, L. Huang, X. Yao, *Adv. Mater.* **2023**, *35*, 2211047.

[128] N. Zhang, Q. He, L. Zhang, J. Zhang, L. Huang, X. Yao, *Adv. Mater.* **2024**, *36*, 8903.

[129] H. Ahmad, H. M. Haseeb, A. Shabbir, Z. S. Khan, N. Toor, G. Ali, *Energy Storage* **2024**, *6*, e619.

[130] H. Kwak, J.-S. Kim, D. Han, J. S. Kim, J. Park, G. Kwon, S.-M. Bak, U. Heo, C. Park, H.-W. Lee, *Nat. Commun.* **2023**, *14*, 2459.

[131] Y. Sakamoto, A. Ishii, T. Shiratori, I. Oikawa, H. Takamura, *Electrochim. Acta* **2023**, *457*, 142488.

[132] S. Payandeh, D. Rentsch, Z. Łodziana, R. Asakura, L. Bigler, R. Černý, C. Battaglia, A. Remhof, *Adv. Funct. Mater.* **2021**, *31*, 2010046.

[133] Z. Min, C. Yang, G.-H. Zhong, Z. Lu, *ACS Appl. Mater. Interfaces* **2022**, *14*, 18373–18382.

[134] A. P. Maltsev, I. V. Chepkasov, A. G. Kvashnin, A. R. Oganov, *Crystals* **2023**, *13*, 756.

[135] W. Zhang, V. Koverga, S. Liu, J. Zhou, J. Wang, P. Bai, S. Tan, N. K. Dandu, Z. Wang, F. Chen, J. Xia, H. Wan, X. Zhang, H. Yang, B. L. Lucht, A.-M. Li, X.-Q. Yang, E. Hu, S. R. Raghavan, A. T. Ngo, C. Wang, *Nature Energy* **2024**, *9*, 386–400.

[136] H. Peng, T. Long, J. Peng, H. Chen, L. Ji, H. Sun, L. Huang, S. G. Sun, *Adv. Energy Mater.* **2024**, *14*, 2400428.

Batteries & Supercaps

Review
doi.org/10.1002/batt.202400432

Chemistry Europe
European Chemical
Societies Publishing

[137] K. Khan, M. B. Hanif, H. Xin, A. Hussain, H. G. Ali, B. Fu, Z. Fang, M. Motola, Z. Xu, M. Wu, *Small* **2024**, *20*, 2305772.

[138] X. Fan, Y. Zhou, M. Wang, J. Lai, W. Shan, Z. Xing, H. Tang, G. Dai, G. Zhang, L. Tan, *ACS Appl. Mater. Interfaces* **2024**, *16*, 17587–17597.

[139] L. Song, R. Li, H. Zhu, Z. Li, G. Liu, Z. Peng, X. Fan, X. Yao, *Adv. Mater.* **2024**, *36*, 2400165.

[140] J. Wegner, S. Ceylan, A. Kirschning, *Chem. Commun.* **2011**, *47*, 4583–4592.

[141] S. S. Kistler, *Nature* **1931**, *127*, 741–741.

[142] R. Roy, *J. Am. Ceram. Soc.* **1969**, *52*, 344–344.

[143] H. Scholze, *J. Non-Crystalline Solids* **1984**, *63*, 1–299.

[144] Y. Dimitriev, Y. Ivanova, R. Iordanova, *J. Univ. Chem. Technol. Metall.* **2008**, *43*, 181–192.

[145] D. Bokov, A. Turki Jalil, S. Chupradit, W. Suksatan, M. Javed Ansari, I. H. Shewael, G. H. Valiev, E. Kianfar, *Adv. Mater. Sci. Eng.* **2021**, *2021*, 1–21.

[146] Z. Wang, Z. Du, L. Wang, G. He, I. P. Parkin, Y. Zhang, Y. Yue, *Nano Energy* **2024**, *121*, 109250.

[147] U. M. Attia, *Crit. Rev. Solid State Mater. Sci.* **2021**, *46*, 587–610.

[148] B. Karmakar, *Glass Nanocomposites*, Elsevier, **2016**, 3–53.

[149] M. S. J. Hashmi, *Comprehensive Materials Processing*, Newnes **2014**.

[150] C. De las Casas, W. Li, *J. Power Sources* **2012**, *208*, 74–85.

[151] J. S. Benjamin, *Metall. Trans.* **1970**, *1*, 2943–2951.

[152] J. S. Benjamin, M. Bomford, *Metall. Trans. A* **1977**, *8*, 1301–1305.

[153] R. Agrawal, G. Pandey, *J. Phys. D* **2008**, *41*, 223001.

[154] D. Fenton, *Polymer* **1973**, *14*, 589.

[155] X. Chen, P. M. Vereecken, *Adv. Mater. Interfaces* **2019**, *6*, 1800899.

[156] Y. Zhao, S. He, L. Li, *Crystals* **2022**, *12*, 805.

[157] Y. Zhang, L. Zhang, C. Zhou, *Acc. Chem. Res.* **2013**, *46*, 2329–2339.

[158] N. Selvakumar, H. C. Barshilia, *Sol. Energy Mater. Sol. Cells* **2012**, *98*, 1–23.

[159] A. Asatekin, M. C. Barr, S. H. Baxamusa, K. K. Lau, W. Tenhaeff, J. Xu, K. K. Gleason, *Mater. Today* **2010**, *13*, 26–33.

[160] A. Carlson, A. M. Bowen, Y. Huang, R. G. Nuzzo, J. A. Rogers, *Adv. Mater.* **2012**, *24*, 5284–5318.

[161] L. Li, Q. Lin, M. Tang, A. J. Duncan, C. Ke, *Chem. A Eur. J.* **2019**, *25*, 10768–10781.

[162] a) C. Xu, B. Quinn, L. L. Lebel, D. Therriault, G. L'Espérance, *ACS Appl. Mater. Interfaces* **2019**, *11*, 8499–8506; b) R. L. Truby, J. A. Lewis, *Nature* **2016**, *540*, 371–378.

[163] J. A. Lewis, *Adv. Funct. Mater.* **2006**, *16*, 2193–2204.

[164] Y. He, F. Yang, H. Zhao, Q. Gao, B. Xia, J. Fu, *Sci. Rep.* **2016**, *6*, 29977.

[165] E. B. Secor, *Flexible Printed Electron.* **2018**, *3*, 035002.

[166] Z. Zhao, X. Tian, X. Song, *J. Mater. Chem. C* **2020**, *8*, 13896–13917.

[167] F. P. Melchels, J. Feijen, D. W. Grijpma, *Biomaterials* **2010**, *31*, 6121–6130.

[168] M. Saadi, A. Maguire, N. T. Pottackal, M. S. H. Thakur, M. M. Ikram, A. J. Hart, P. M. Ajayan, M. M. Rahman, *Adv. Mater.* **2022**, *34*, 2108855.

[169] J. Cesarano, S. Grieco, *Materials Technology* **1997**, *12*, 98–100

[170] J. A. Lewis, J. E. Smay, J. Stuecker, J. Cesarano, *J. Am. Ceram. Soc.* **2006**, *89*, 3599–3609.

[171] M. Seiti, O. Degryse, R. M. Ferraro, S. Giliani, V. Bloemen, E. Ferraris, *Int. J. Bioprint.* **2023**, *9*, 57–74.

[172] C. Cooper, B. Hughes, *2020 Pan Pacific Microelectronics Symposium (Pan Pacific)*, IEEE, **2020**, 1–11.

[173] a) H. S. Ghazali, E. Askari, Z. S. Ghazali, S. M. Naghib, T. Braschler, *Colloid Interface Sci. Commun.* **2022**, *50*, 100667; b) J. Stampfl, M. Schwentenwein, J. Homa, F. B. Prinz, *MRS Commun.* **2023**, *13*, 1–9

[174] G. Katal, N. Tyagi, A. Joshi, *Int. J. Sci. Res.* **2013**, *3*, 2250–3153.

[175] P. F. Jacobs, *Rapid Prototyping & Manufacturing: Fundamentals of Stereolithography*, Society of Manufacturing Engineers **1992**.

[176] K. Wang, W. Zou, B. Quan, A. Yu, H. Wu, P. Jiang, Z. Wei, *Adv. Energy Mater.* **2011**, *1*, 1068–1072.

[177] a) P. Bartolo, J. Gaspar, *CIRP Ann.* **2008**, *57*, 235–238; b) W. K. Swainson, Google Patents, **1977**.

[178] J. Huang, Q. Qin, J. Wang, *Processes* **2020**, *8*, 1138.

[179] J. R. Tumbleston, D. Shirvanyants, N. Ermoshkin, R. Janusziewicz, A. R. Johnson, D. Kelly, K. Chen, R. Pinschmidt, J. P. Rolland, A. Ermoshkin, *Science* **2015**, *347*, 1349–1352.

[180] J. Wu, L. Shen, Z. Zhang, G. Liu, Z. Wang, D. Zhou, H. Wan, X. Xu, X. Yao, *Electrochem. Energy Rev.* **2021**, *4*, 101–135.

[181] J. Janek, W. G. Zeier, *Nat. Energy* **2016**, *1*, 1–4.

[182] J. Wu, S. Liu, F. Han, X. Yao, C. Wang, *Adv. Mater.* **2021**, *33*, 2000751.

[183] P. Bron, S. Johansson, K. Zick, Schmedt auf der Günne, S. Dehnen, B. Roling, *J. Am. Chem. Soc.* **2013**, *135*, 15694–15697.

[184] a) B. Neudecker, N. Dudney, J. Bates, *J. Electrochem. Soc.* **2000**, *147*, 517; b) W.-Y. Liu, Z.-W. Fu, Q.-Z. Qin, *J. Electrochem. Soc.* **2007**, *155*, A8.

[185] Z. Gao, H. Sun, L. Fu, F. Ye, Y. Zhang, W. Luo, Y. Huang, *Adv. Mater.* **2018**, *30*, 1705702.

[186] Q. Zhao, S. Stalin, C. Zhao, L. Archer, *Nat. Rev. Mater.* **2020**, *5*, 229–252.

[187] a) Y. Cao, M. Li, J. Lu, J. Liu, K. Amine, *Nat. Nanotechnol.* **2019**, *14*, 200–207; b) Z. Lin, T. Liu, X. Ai, C. Liang, *Nat. Commun.* **2018**, *9*, 5262

[188] A. Sharafi, S. Yu, M. Naguib, M. Lee, C. Ma, H. M. Meyer, J. Nanda, M. Chi, D. J. Siegel, J. Sakamoto, *J. Mater. Chem. A* **2017**, *5*, 13475–13487.

[189] L. Cheng, E. J. Crumlin, W. Chen, R. Qiao, H. Hou, S. F. Lux, V. Zorba, R. Russo, R. Kostecki, Z. Liu, *Phys. Chem. Chem. Phys.* **2014**, *16*, 18294–18300.

[190] Y. Liang, H. Liu, G. Wang, C. Wang, Y. Ni, C. W. Nan, L. Z. Fan, *InfoMat* **2022**, *4*, e12292.

[191] S. Chen, D. Xie, G. Liu, J. P. Mwizerwa, Q. Zhang, Y. Zhao, X. Xu, X. Yao, *Energy Storage Mater.* **2018**, *14*, 58–74.

[192] P. Wang, W. Qu, W. L. Song, H. Chen, R. Chen, D. Fang, *Adv. Funct. Mater.* **2019**, *29*, 1900950.

[193] M. Armand, J.-M. Tarascon, *Nature* **2008**, *451*, 652–657.

[194] A. Banerjee, X. Wang, C. Fang, E. A. Wu, Y. S. Meng, *Chem. Rev.* **2020**, *120*, 6878–6933.

[195] L. R. Mangani, C. Villevieille, *J. Mater. Chem. A* **2020**, *8*, 10150–10167.

[196] M. Park, X. Zhang, M. Chung, G. B. Less, A. M. Sastry, *J. Power Sources* **2010**, *195*, 7904–7929.

[197] R. Koerver, W. Zhang, L. De Biasi, S. Schweidler, A. O. Kondrakov, S. Kolling, T. Brezesinski, P. Hartmann, W. G. Zeier, J. Janek, *Energy Environ. Sci.* **2018**, *11*, 2142–2158.

[198] T. K. Schwietert, V. A. Arszelewska, C. Wang, C. Yu, A. Vasileiadis, N. J. de Klerk, J. Hageman, T. Hupfer, I. Kerkamm, Y. Xu, *Nat. Mater.* **2020**, *19*, 428–435.

[199] K. H. Kim, Y. Iriyama, K. Yamamoto, S. Kumazaki, T. Asaka, K. Tanabe, C. A. Fisher, T. Hirayama, R. Murugan, Z. Ogumi, *J. Power Sources* **2011**, *196*, 764–767.

[200] J. B. Goodenough, Y. Kim, *Chem. Mater.* **2010**, *22*, 587–603.

[201] J. L. Barton, J. O. M. Bockris, *Proc. R. Soc. London Ser. A* **1962**, *268*, 485–505.

[202] F. Han, A. S. Westover, J. Yue, X. Fan, F. Wang, M. Chi, D. N. Leonard, N. J. Dudney, H. Wang, C. Wang, *Nat. Energy* **2019**, *4*, 187–196.

[203] S. Wang, H. Xu, W. Li, A. Dolocan, A. Manthiram, *J. Am. Chem. Soc.* **2018**, *140*, 250–257.

[204] M. J. Wang, R. Choudhury, J. Sakamoto, *Joule* **2019**, *3*, 2165–2178.

[205] J. M. Doux, H. Nguyen, D. H. Tan, A. Banerjee, X. Wang, E. A. Wu, C. Jo, H. Yang, Y. S. Meng, *Adv. Energy Mater.* **2020**, *10*, 1903253.

[206] a) Y. Han, S. H. Jung, H. Kwak, S. Jun, H. H. Kwak, J. H. Lee, S. T. Hong, Y. S. Jung, *Adv. Energy Mater.* **2021**, *11*, 2100126; b) C. Wang, R. Yu, S. Hwang, J. Liang, X. Li, C. Zhao, Y. Sun, J. Wang, N. Holmes, R. Li, *Energy Storage Mater.* **2020**, *30*, 98–103.

[207] X. Liu, B. Zheng, J. Zhao, W. Zhao, Z. Liang, Y. Su, C. Xie, K. Zhou, Y. Xiang, J. Zhu, *Adv. Energy Mater.* **2021**, *11*, 2003583.

[208] N. Ohta, K. Takada, I. Sakaguchi, L. Zhang, R. Ma, K. Fukuda, M. Osada, T. Sasaki, *Electrochem. Commun.* **2007**, *9*, 1486–1490.

[209] a) K. B. Hatzell, X. C. Chen, C. L. Cobb, N. P. Dasgupta, M. B. Dixit, L. E. Marbella, M. T. McDowell, P. P. Mukherjee, A. Verma, V. Viswanathan, *ACS Energy Lett.* **2020**, *5*, 922–934; b) T. Krauskopf, F. H. Richter, W. G. Zeier, J. r. Janek, *Chem. Rev.* **2020**, *120*, 7745–7794; c) H. Liu, X.-B. Cheng, J.-Q. Huang, H. Yuan, Y. Lu, C. Yan, G.-L. Zhu, R. Xu, C.-Z. Zhao, L.-P. Hou, *ACS Energy Lett.* **2020**, *5*, 833–843.

[210] W. Huang, Z. Bi, N. Zhao, Q. Sun, X. Guo, *Chem. Eng. J.* **2021**, *424*, 130423.

[211] F. Han, J. Yue, X. Zhu, C. Wang, *Adv. Energy Mater.* **2018**, *8*, 1703644.

[212] M. Jäckle, K. Helmbrecht, M. Smits, D. Stottmeister, A. Groß, *Energy Environ. Sci.* **2018**, *11*, 3400–3407.